Upon the effect of Zn during friction stir welding of aluminum-copper and aluminum-brass systems

Marie-Noëlle Avettand-Fènoël, T. Nagaoka, Maya Marinova, Roland Taillard

Upon the effect of Zn during friction stir welding of aluminum-copper and aluminum-brass systems.

M.-N. Avettand-Fènoël [a*], T. Nagaoka [b], M. Marinova [c], R. Taillard [a]

a: Univ. Lille, CNRS, INRAE, Centrale Lille, UMR 8207 – UMET - Unité Matériaux Et Transformations, F-59000 Lille, France

b: Osaka Research Institute of Industrial Science and Technology, Osaka 5368553, Japan

c: Univ. Lille, CNRS, INRA, Centrale Lille, Univ. Artois, FR 2638 – IMEC – Institut Michel-Eugène Chevreul, F-59000 Lille, France

* Corresponding author – E-mail: marie-noelle.avettand-fenoel@univ-lille.fr
Tel: 33(0)320436927

Abstract

The present study deals with the effect of Zn on the linear friction stir lap welding of Al to Cu or to brass with a pinless tool. Zn was considered either as a filler metal or as an element in solid solution in α-brass. The lap joint configuration with a groove machined at the top of the bottom plate was chosen in order to test for the first time the influence of liquid Zn at the interface in case of melting by avoiding its ejection. Besides, the use of a pin free tool to join three millimeters thick plates is challenging. The paper presents and discusses the macrostructure and microstructure of the various joints together with their mechanical properties. A strong emphasis is given to the lubricating action of a liquid phase on the material flow as well as on the mechanisms of phase transformations at the various interfaces. The present work reports an early investigation of the material flow in linear friction stir lap welding with a pinless tool. The lap shear tensile fracture behavior of the welds is related to their interface morphology and microstructure. In particular, the fairly good shear resistance of the brass-Zn-Al joint arises from the composite nature of its interface despite its flatness and high thickness.

Keywords

Friction stir welding; aluminum, brass, copper and zinc interlayer; interface; material flow; microstructure; phase transformations; mechanical properties.

1. Introduction

Aluminum-copper and aluminum-brass joints present some interest in particular for thermal and electrical applications. However, Al and Cu have a high chemical affinity for each other which generally leads to the formation of Al_xCu_y intermetallic compounds (IMCs) during welding **[1-3]**. Although these IMCs ensure metallurgical bonding between the materials, they are at once brittle and bad thermal and electrical conductors, which is detrimental to the mechanical and functional performances of the Al-Cu joints **[4]**. Besides, the IMCs formation is promoted at the liquid state because of the important diffusion of the elements. It is the reason why lots of studies focused on solid state welding of such materials, among which friction stir welding (FSW), since the hampering of the IMCs formation should

be enhanced by the short welding time. Nevertheless, some IMCs still continue to form **[2]**. Various solutions have then been reported in the literature in order to limit or to suppress the IMCs formation at the joint interface, namely:

(i) Water cooling along friction stir welding was proved to restrain the total thickness of the Al_2Cu and Al_4Cu_9 layers below 2 µm. This width is reduced by an order of magnitude compared to conventional friction stir welding **[5]**;

(ii) The application of ultrasounds during friction stir welding was shown to enlarge the deformed volume around the pin because of material softening. This increase of material flow decreases the IMCs thickness and leads to improved mechanical properties of the joint **[6-7]**;

(iii) The use of a smooth cylindrical pin instead of a pin with threads and/or flutes was proved to lead to a thinner IMCs layer since the peak temperature was lower **[8]**;

(iv) The intercalation of a Zn layer ~~in ultrasounds welding of~~ between Al ~~to~~ and Cu joined by ultrasounds welding led to a 40 µm thick joint interface containing an Al-Zn eutectic and $CuZn_5$ particles with an improved shear lap tensile strength **[9]**. Again in the case of ultrasound welding of Al and Cu, a Zn-3Al interlayer entailed the formation of a $Al_{4.2}Cu_{3.2}Zn_{0.7}$ (τ) phase which behaves as a diffusion barrier between Al and Cu ~~resulting~~ and therefore results in improved mechanical properties of the joint **[10]**. A thin Zn filler intercalated between Al and Cu during ~~basic~~ conventional FSW was shown to increase the ultimate tensile strength of the joints by a factor 3 compared to Zn free joints **[11]**.

Various explanations of the beneficial effect of Zn during Al to Cu FSW have been proposed. They consist for instance in (i) an interface heating due to the presence of liquid Zn, (ii) the replacement of the brittle Al_xCu_y intermetallic compounds by other phases, (iii) a catalytic action of Zn on the reactions between Al and Cu, (iv) the interface cleaning by liquid Zn etc. These controversial explanations are however questioned according to the frequent ejection of liquid Zn from the joint interface during friction stir welding. ~~According to this short overview, it is therefore logical to question about the existence of an another and more unified understanding of the real effect of Zn during FSW. Given the controversial explanation related to the effect of the Zn action during Al to Cu FSW of Al-Cu supplied in literature,~~ It seems therefore relevant to analyze the true effect of liquid Zn by trying to keep it at the joints interface by means of a groove at the top of the bottom plate.

The present study tackles this question by means of Al-Cu and Al-brass friction stir welded joints in presence or not of a Zn filler. The 30 at% Zn content of brass was chosen so as to not exceed the solubility of Zn in Cu whatever the temperature **[1]**. The paper thus aims

(i) to investigate the behavior and the role of Zn during welding, namely does Zn enter in solid solution in the parent materials (Cu, brass and Al), or does it rather form either intermetallic compounds with Al and Cu or eutectic constituents? The importance of the primitive state of Zn either in solid solution as in the brass, or as an easily fusible element in a pure Zn filler will also be investigated;

(ii) to consider the consequences of the changes of microstructure due to Zn on the joint mechanical performances.

Another point of interest of the current work stems from the use of a pinless tool during welding in place of the conventional pin ones employed to get the Al-Cu linear lap friction stirred joints up to now considered in the literature; indeed, a unique study dealing with Al-Cu linear lap friction stir welding with a stepped configuration, a Zn interlayer and a pinless tool has been reported in literature **[12]**. This change of tool shape is expected to improve the joint mechanical resistance as it reduces the heat input **[13-15]** and mechanical mixing **[16]** which should reduce the size and extent of the brittle intermetallic compounds

during friction stir welding. The 3 mm thickness of the present blanks is however a challenge as the beneficial effects of pinless tools are often obtained for the friction stir spot welding or butt friction stir welding of 1 to 1.5 mm thin sheets **[13, 17-19]** and very scarcely with thicker plates **[12]**. As a matter of fact, as the thickness increases, the shoulder influence becomes ever more localized ~~to~~ at the top sheet surface.

2. Experimental procedure

The base materials, whose chemical compositions are summarized in table 1, were pure aluminum AA1050 ($HV_{0.05}$ = 43.7), oxygen free copper C1020 ($HV_{0.05}$ = 79) and single phased α-brass C2600 ($HV_{0.05}$ = 121). The 3 mm thick plates are 100 mm wide and 200 mm long. The roughness of the AA1050, C1020, C2600 and Zn plates are respectively 0.10, 0.06, 0.09 and 0.19 µm.

In some cases, two stacked 100 µm thick Zn layers were inserted inside a 0.2 mm deep and 20 mm wide groove cut at the top surface of the bottom plate in the assembly. The groove was machined in order to avoid Zn ejection from the joint area in case of Zn melting.

Table 1: Nominal composition (mass. %) of the AA1050, C1020 and C2600 base materials.

Material	Al	Cu	Sn	Zn	Ni	Fe	Pb	Si	Mg	Mn	Ti	V	Other
AA1050	99.5 min	0.05 max	-	0.05 max	-	0.4 max	-	0.25 max	0.05 max	0.05 max	0.03	0.05	-
C1020	-	99.96 min	-	-	-	-	-	-	-	-	-	-	-
C2600	<0.02	Balance	<0.05	30	<0.2	<0.05	<0.005	-	-	-	-	-	<0.1

The blanks were clamped on a plain steel backing plate. They were friction stir welded in an overlap configuration (figure 1) with a pinless tool made of H13 tool steel. A surface with a 10° angle of concavity was machined across the outer half of the shoulder radius (figure 2) so as to prevent an ejection of material on the plate surface at the borders of the tool during welding **[20]**. The 18 mm diameter tool was 3° backwards tilted. Welding was performed ~~in~~ by controlled displacement with a tool penetration depth of 0.2 mm and the axial down force was continuously measured. The welding rate (v) was 200 mm/min. For the joints with aluminum at the top (joints 1 to 3), the clockwise rotational speed (ω) was 1500 rpm while it was 2000 rpm for the joint with brass at the top (joint 4). The latter experiment was performed in order to take advantage of the location of a stronger material at the top of the joint owing to the Zn behavior at the Al-Zn-Cu joint interface. In addition, so as to measure the thermal welding cycle, a K-type thermocouple with a 0.5 mm diameter was set across the thickness of the backing plate with its tip at the contact with the back of the bottom plate centre just under the location of the shoulder at the top surface.

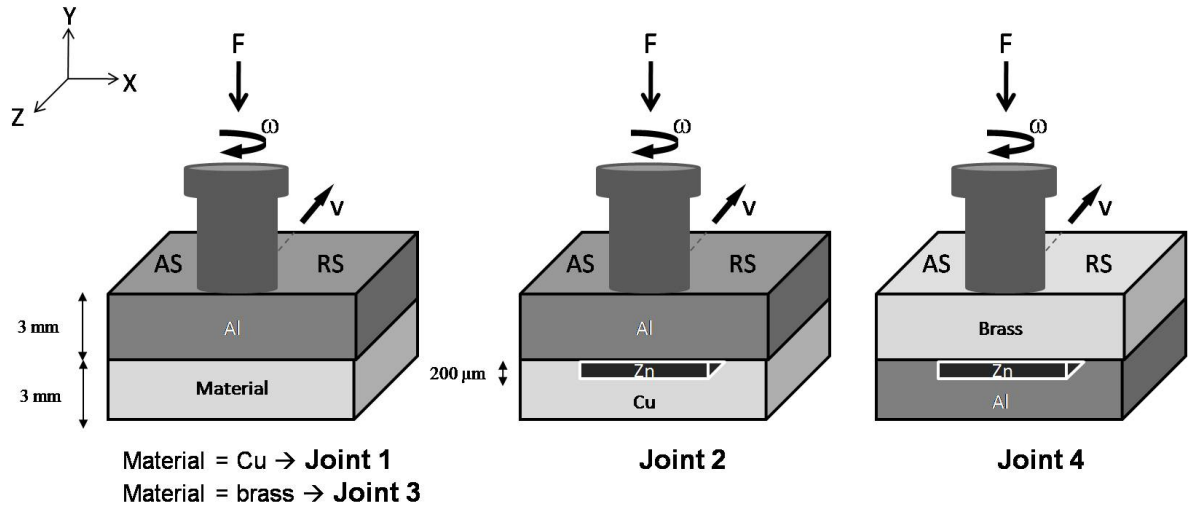

Figure 1: Configurations of the different joints.

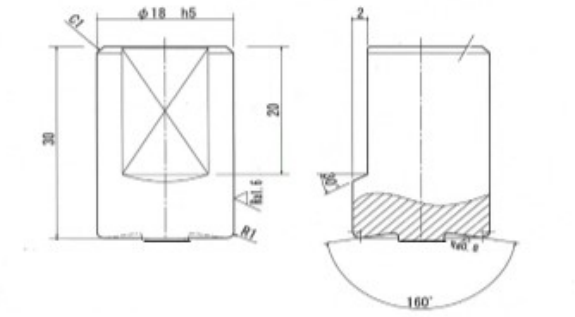

Figure 2: Schematics and dimensions of the welding tool (the dimensions are given in mm).

2.1. Microstructural characterization

The specimens were grinded with different grades of SiC papers and finally polished with a 1 µm sized diamond paste.

The samples were analyzed by light microscopy and scanning electron microscopy (FEG/SEM) with the secondary electron (SE) or back scattering electron (BSE) mode and with X-ray energy dispersive spectroscopy (EDX).

A thin foil cut across the interface of the Al-Cu joint was prepared by focused ionic beam (FIB) and analyzed by high resolution transmission electron microscopy (HRTEM) and STEM-EDX.

Some X-ray diffractometry analyses were also performed on the (X,Y) plane of the samples (figure 1). These experiments were achieved in a Bragg-Brentano configuration and using a Co anticathode with a wavelength of 1.78901 Å.

2.2. Mechanical characterization

With regard to the mechanical properties, Vickers microhardness measurements under a load of 50 g were performed on the joints transverse cross section (X-Y plane) every 500 µm along the X axis and every 1 mm along the Y axis (figure 1).

Two or three shear-tensile tests per joint configuration were performed according to the JIS Z3136 standard with a displacement rate of 1 mm/min. The samples were cut by wire electrical discharge machining in the (X,Z) joints transverse section with the orientation and

dimensions indicated in figure 3. As it is the rule in welding, the tensile tests were conducted in order to get a quick insight of the suitability of the process setting.

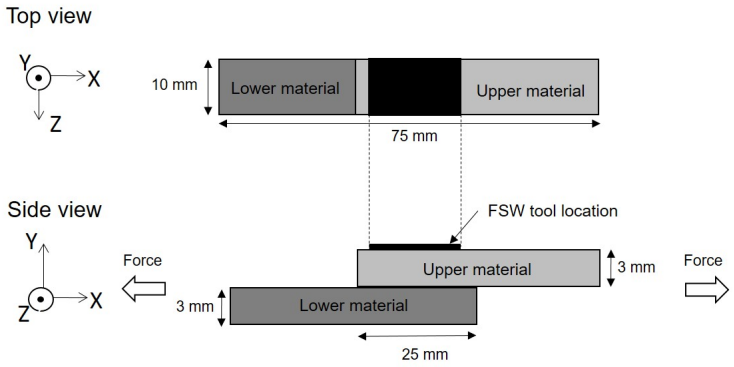

Figure 3: Dimensions of the shear-tensile specimens.

3. Results

3.1 Thermal cycles and load cycles during welding *vs.* macroscopic surface features of the joints

The thermal cycles and load cycles recorded during welding are displayed in figure 4 while the joints surfaces are shown in figure 5. For the joint configuration with Al at the top, the peak temperature recorded at the joint bottom plate remained in-between 250 and 375°C. It is worth noting that the peak temperature was far smaller in presence of a Zn interlayer (figures 4a, b, c). The cooling rates were comprised between 6.8 (for the Al-Zn-Cu joint) and 9.7 K/s (for the Al-brass joint) (figures 4a to c). Concerning the load applied on the tool during the FSW stage, which lasted around 20 s, it was close to 5000 N for the Al-Cu joint, and to 3000 N for the Al-brass and Al-Zn-Cu welds (figures 4e, f, g). During the welding stage, the down force continuously decreased for the Al-Cu joint while it remained constant for the Al-brass weld (figures 4e and f). These evolutions agree with the reduction of the Cu mechanical strength at the welding temperature. In contrast with the previous cases of joining, the Al-Zn-Cu welding occurs with successive and important drops and peaks of loads (figure 4g). In agreement with these discontinuities of tool loading, the top surface of the Al-Zn-Cu joint presents a ragged macrostructure which contrasts with its smoothness for the other joints (figures 5a, b, c).

In the case of the joint with brass at the top, the peak temperature was 477.6°C and thus far higher than those obtained for the other configurations (figure 4d). This result is consistent with the higher melting temperature of brass compared to that of Al and with the 0.6-0.7 homologous temperature (i.e. ~~the ratio of the~~ absolute welding temperature ~~to and~~ divided by the absolute melting point) required for the plasticization of the material and necessary to the tool advance. The cooling rate of this joint was thus higher than those of the other joints (figures 4a to d). The force applied on the tool was around 4000 N and ~~low magnitude~~ small oscillations of the load are noticed during the stationary welding stage (figure 4h), which agrees with the pretty smooth surface of the weld (figure 5d).

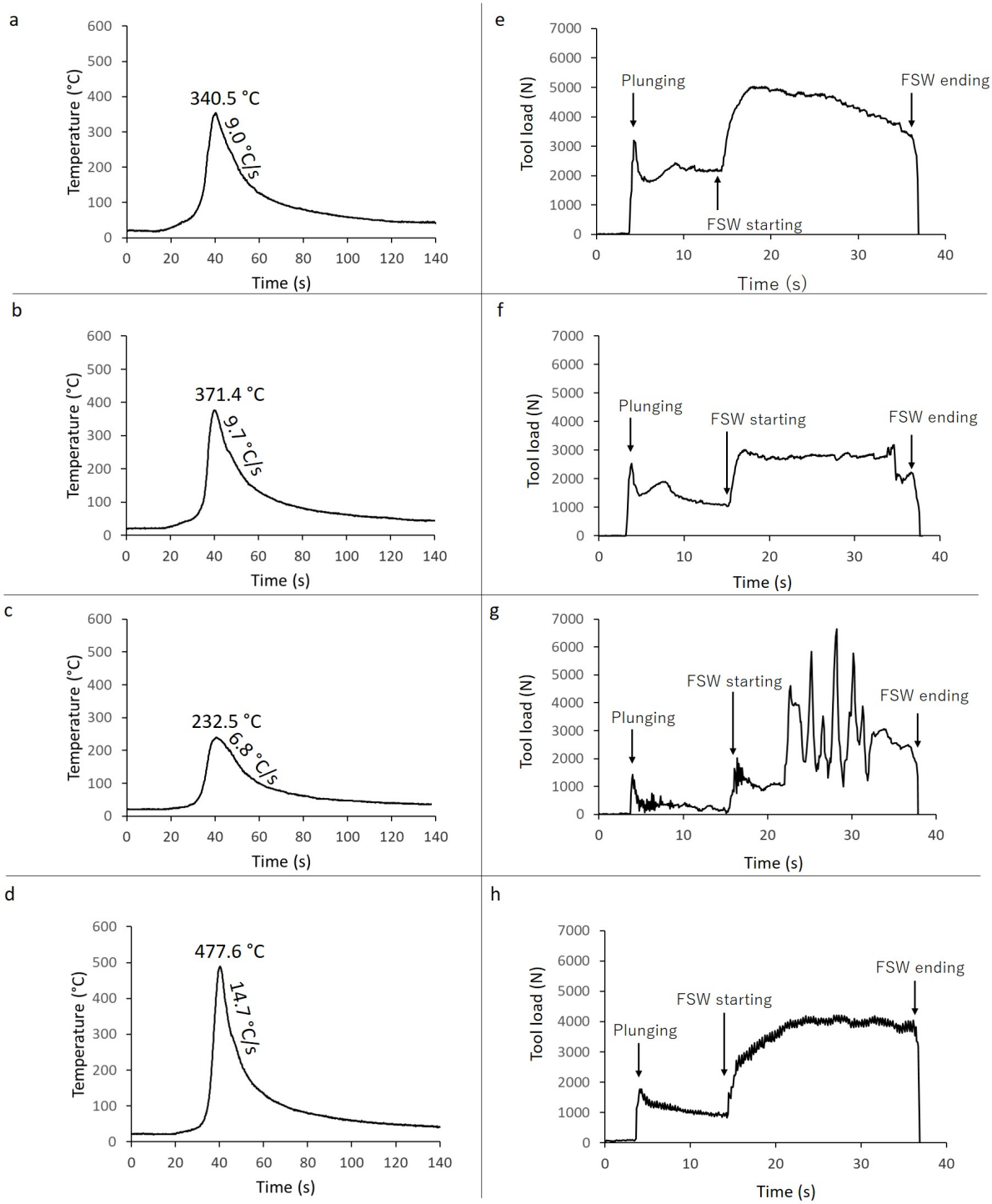

Figure 4: Thermal and axial load cycles for an Al-Cu (a and e, respectively), Al-brass (b and f, respectively), Al-Zn-Cu (c and g, respectively) and brass-Zn-Al (d and h, respectively) joint during welding. The time scales are not synchronized, as temperature is registered at some place along the seam contrary to the down force which was continuously measured during welding.

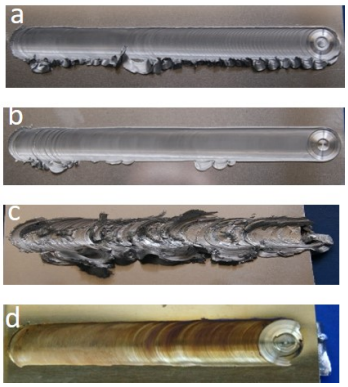

Figure 5: Aspect of the top surface of the Al-Cu (a), Al-brass (b), Al-Zn-Cu (c) and Brass-Zn-Al (d) joints.

3.2 Joints structure

Concerning the Al-Cu joint, the welding interface has remained essentially flat with no penetration of the top sheet into the bottom plate. Not any deformation feature was further noticed within the surrounding base materials at the scale of light microscopy (not shown here). The interface is further discontinuous as it is constituted of discrete particles with a 50 nm to 1 µm thickness and a length in-between 100 and 200 nm (see yellow arrows in figure 6a). Figures 6b, c and d show that the interfacial particles are polycrystalline as they contain 7 nm sized grains of Al_4Cu_9. This composition is consistent with the EDX analyses (not shown here) which indicate a Cu/Al atomic ratio in-between 2 and 3. X-ray diffraction confirms the presence of this compound together with AlCu, Al_2Cu and Al_2Cu_3 phases (figure 6e).

The Al-brass joint interface is also macroscopically flat (not shown here). At the micrometer scale, it contains a continuous layer between the parent materials (figure 7a). This intermediate layer is characterized by a rather straight interface with the Al base material, which very likely corresponds to the Al – brass primitive interface. The other interface of the intermediate layer with brass is wavier (figure 7). The latter observation is consistent with crystals growth from the faying interface towards brass. The intermediate layer is 15 µm thick on average. From brass to Al, it is successively made of (i) a 4 µm thick layer (sublayer 1) with a 14%Al - 46%Cu - 38%Zn average composition, (ii) a 2.5 µm thick zone (sublayer 2) with the 52%Al – 39%Cu – 9%Zn mean composition, which is close to that of $Al_{4.2}Cu_{3.2}Zn_{0.7}$ (τ'), (iii) an Al_2Cu–phase containing about 2.0 to 4.6 at.% Zn in solid solution over a 8 µm thickness (sublayer 3 with a grey contrast in figure 7a) and (iv) a 3 µm thick layer (sublayer 4) with the 68.4%Al-21%Cu-10.6%Zn mean composition (figure 7e). These results are consistent with the X-ray diffractometry analyses, which identified γ-Cu_5Zn_8 (sublayer 1) and τ'(sublayer 2) which both exist over a large composition domain according to the phase diagrams, as well as the Al_2Cu (sublayer 3) compounds in the joint (figure 7f). Both outermost sublayers are enriched in Zn in particular on the brass side (figure 7d and e).

For the Al-Zn-Cu joint, it is worth noting the crushing of the Zn layer at the joint interface (see yellow arrow in figure 8a). The Al-Zn interface is deflected over a width corresponding to the diameter of the central flat part of the tool tip (see figure 2). This incurved part of the Al-Zn interface is also ragged at some places (figures 8a and 8a'). Beneath this zone, the upper surface of the Cu bottom plate is far less indented (figure 8a). The almost quasi complete squeezing of the pure Zn interlayer at the interface along the joint center line (figures 8a and d) is due to the concomitant effect of the pressure exerted by the tool on liquid Zn during welding and of the occurrence of Al-Zn phase transformations at the interface. In fact, some biphased dendrites (figures 8h and k) and some multiphased

constituents are observed at and close to the interface (figures 8f, h and j) and even at the top surface (figures 8i, k and l). In accordance with the EDX profile in figure 8g, figures 8h and k indeed display dendrites of primary solid that have undergone the Zn-Al eutectoid transformation during cooling. Point 1, figure 8 is in fact very close to the eutectoid composition. These dendrites are embedded in a eutectic matrix (point 2, figure 8) whose Al rich constituent has itself experienced the eutectoid transformation during cooling. Such a microstructure reveals the slightly hypoeutectic composition of the primitive liquid phase and thus the already marked diffusion of Al in liquid Zn during welding. The Al content of this primitive liquid actually exceeds 11.3 at% Al. The dendrites are surrounded by a layer with a low Al content whose micrometric thickness suggests that it has formed at the solid state. A close examination of figures 8h and k suggests that this solute depleted layer has to do with a precipitation phenomenon at the dendrites interface. The existence of these ~~hundred nanometers diameter~~ particles with a diameter of hundred nanometers is consistent with the detection of traces of Cu (figure 8g and figure 8h, points 1 and 2). Figure 8l further shows the eutectic-like microstructure of the Al grain boundaries at the top surface of the weld. The 3 µm diameter of these Al grains markedly differ from the 200 µm average length and 50 µm mean width of the elongated grains of the base Al because of the occurrence of dynamic recrystallization during welding. Besides, some Al-Zn contamination has also been curiously observed at the tool surface. The latter result seems to be correlated with the significant load fluctuations recorded during welding (figure 4g) which are due to the successive slipping and sticking of the tool on the weld surface because of the local emergence of liquid Zn at this place. In accordance with this observation, numerous Zn rich material stream lines (figures 8a-d, f and j) are noticed across the whole thickness of the upper Al plate. These flow lines are contained in a basin shaped welding zone (delineated in yellow in figure 8a'). Such an asymmetrical shape of welding zone is commonly observed in linear friction stir welding while using conventional pin tools **[21-22]**. It has however never been generated with a pinless tool as, according to the authors' knowledge, a pin free tool has hitherto only been used for stationary friction stir spot welding **[17,23]**. In addition, the shape and distribution of the present stream lines markedly differ from those of the symmetrical onion rings that are generally generated within a FSW nugget by the pin advance **[24]**. This difference is consistent with the absence of probe. It is therefore relevant to investigate the geometry of the Zn-bearing stream lines in order to obtain a first insight to the material flow in the Al top plate during linear lap welding with a pin free tool. Figure 8a' clearly confirms the difference of material deformation on either side of an advancing tool **[25-26]** and whatever the depth in the Al plate. Close to the Al top surface, the flow is rather lamellar on the advancing side (AS) as the material is trapped under the tool surface because of the pressure and twist applied by a rotating circular block **[27]** and then extruded owing to the tool advance. Again not far from the Al surface, the flow is on the contrary turbulent on the retreating side (RS) because of the proximity of the prevailing centrifugal ejection of material behind the tool to the centripetal displacement of the material just beneath the tool contact surface. Deeper in the Al plate, the material moves upwards on the AS side where it is again trailed by the tool; but downwards on RS side, the material moves away from the tool. The detection of Fe rich debris originating from the shoulder material, on the fracture surface (point 1, figure 17c) further proves this material downflow across the top plate up to the primitive interface. This downwards ejection of material occurs on a shorter path, the deeper it occurs. The flow is somewhat turbulent at the meeting point (figure 8a') of these opposite directions of material displacement. Some swirls are also generated on the RS side in contact of the welding interface because of the high strength and then far less deformation of the adjoining Cu bottom plate. The comparison between the present results and the material flow in stationary FSSW with a flat featureless pinless tool **[23]** clearly demonstrates the prevailing action of the tool advance. Owing to the

absence of tool travel assisted or not by the tool tilt, pin free FSSW only gives rise to vortices nearby the edges of the tool contact area and to dragging of the underneath material towards the shoulder edge. Contrary to the present observations, material flow was also very reduced at the center of the FSSW weld.

Besides the flow lines, a wormhole defect filled with a Zn rich phase (point 3 in figure 8b) has also been detected on the advancing side in Al and near the faying interface.

It is also worthy to note that the XRD investigations have established the absence of a noticeable amount of the Al_xCu_y, Cu_xZn_y or $Al_xCu_yZn_z$ IMCs. In addition, not any significant diffusion of Zn was detected into the Cu base material (figure 8g).

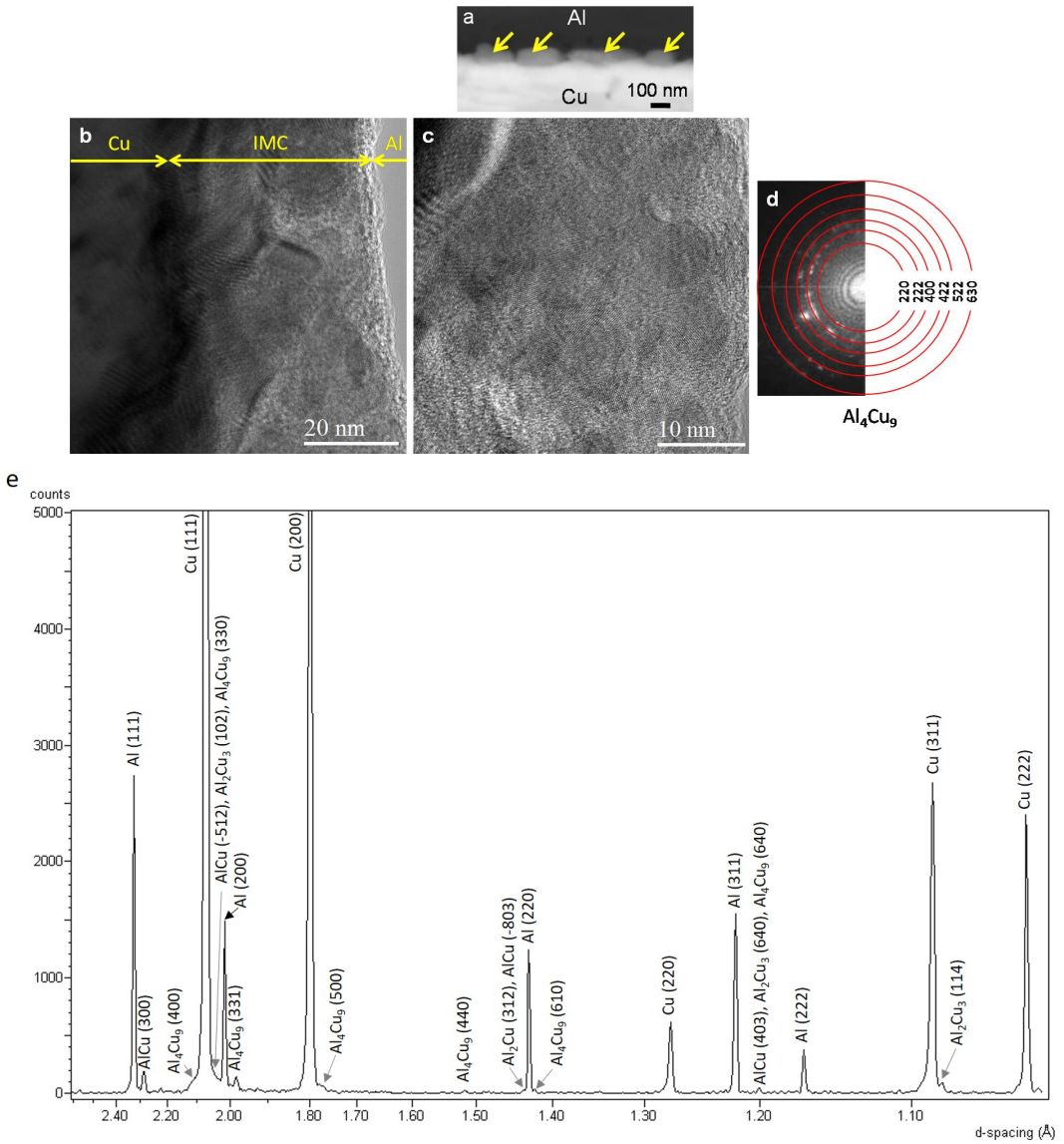

Figure 6: Interface of the Al-Cu joint: SEM (X-Y plane) (a), HRTEM image (Y-Z plane) (b); magnified HRTEM image of the interfacial layer (c) and associated fast Fourier transformation (FFT) (d). X-ray diffraction pattern (e).

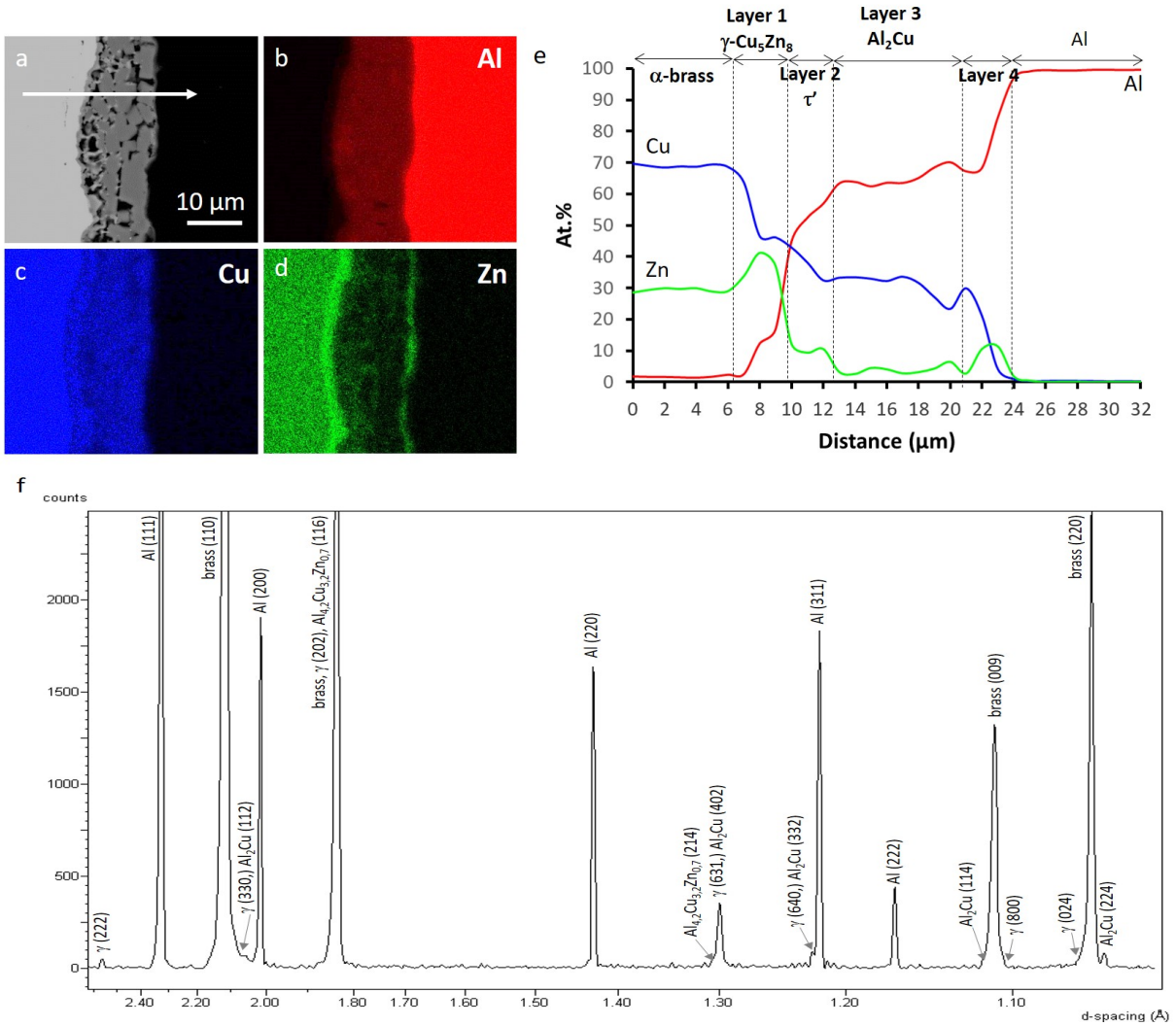

Figure 7: Micrograph of the interfacial zone of the Al-brass joint (BSE/SEM) (a) and associated Al-Kα (b), Cu-Kα (c) and Zn-Kα (d) X-ray maps (EDX). Profile of chemical composition (e) along the line drawn in figure (a) (EDX). It is worth noting that γ-Cu_5Zn_8 exists over a large composition domain according to the phase diagram. X-ray diffraction pattern of the Al-brass joint (f).

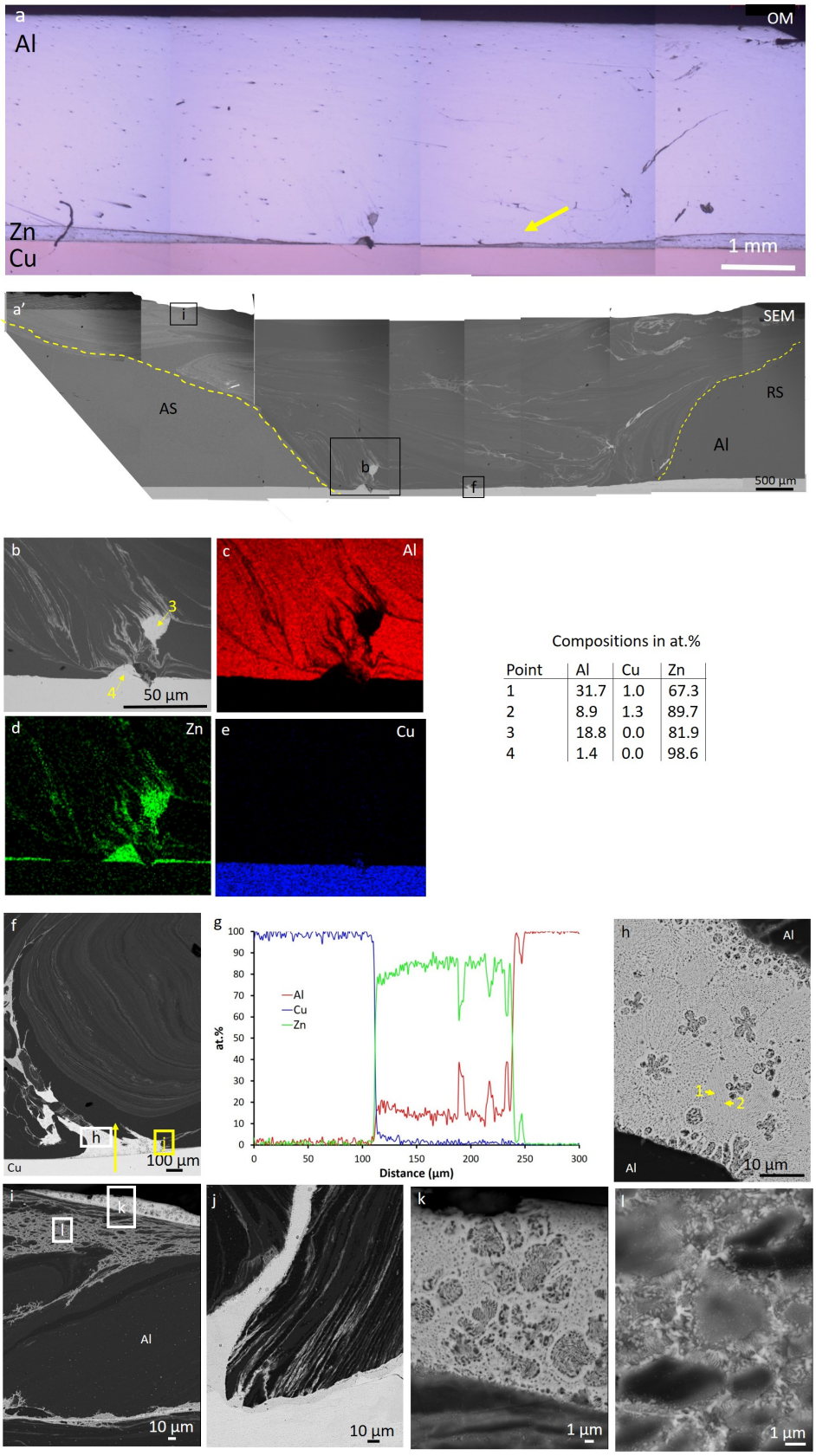

Figure 8: Micrographs of the interfacial zone in a (X,Y) transverse cross section of the Al-Zn-Cu joint: global view (a : OM and a': BSE/SEM), particular zone (b) with associated Al-Kα, Zn-Kα and Cu-Kα X-ray maps (c-e) and other features (f, h-l) (BSE/SEM) with profile of chemical composition (g) along the yellow line drawn in figure (f) (EDX).

The configuration of joint 4 (figure 1) contrasts with that of the former welds, that were characterized by the positioning of the softer plate at the tool contact. On the contrary, for this brass-Zn-Al case, brass which is stronger than Al, and even than Cu, is placed at the top. This new configuration was adopted in order to attempt to keep Zn at the joint interface by preventing its ejection away from the faying plane along the material flow lines dispersed in the total thickness of the upper plate, as in the previous Al-Zn-Cu case (figure 8).

The brass-Zn-Al welding interface is rather flat with a thickness decreasing at the footprint of the tool (see black arrows in figure 9a). The 200 µm thick Zn layer originally placed at the faying interface is indeed replaced by a continuous layer with a thickness in between 60 and 170 µm (figures 9-11). This reduction of thickness very likely results from both the upsetting action of the tool and the phase transformations at the liquid state experienced by the interface as explained in the following. The interface is somewhat wavy on the brass side while it is smoother on the Al side (figure 10a).

~~Different microstructural features are noticed in the~~The interfacial zone just beneath the tool contact area is displayed in ~~(~~figure~~s~~ 9b ~~and c)~~. The interlayer presents dendrites of an oversaturared Zn solid solution containing 46.9 at.% Al and 3 at.% Cu (point 1, figure 11a). The dendrites are more or less equiaxed and coarse and their orientation evolves erratically along the interface. Their global random orientation means that there was not any preferential direction of a rather slow heat exchange at the interface. The dendrites are embedded in a Zn rich layer bearing about 11.0 at.% Al and 11.8 at.% Cu (point 3, figure 10c and point 2, figure 11a). The remaining interdendritic spacings are occupied by a periodic biphased constituent with a global ternary Zn-Al-Cu chemical composition close to that of the binary Zn-Al eutectic (points 3 and 4, figure~~s~~ 11b ~~and c~~).

The wavy interface in contact with brass is bordered by a phase with a thickness of 2.5 µm and a composition of 44.9 at.% Zn, 41.9 at.% Cu and 13.2 at.% Al (point 1, figures 10a and b).

Some polygonal intermetallic compounds with a composition close to Al_2Cu are also observed in the interfacial layer. These particles may also contain some traces of Zn (see for instance point 5 in figure 11c~~d~~)

In the surroundings of the tool location, the interface contains a supersaturated Zn solid solution with a high Al content over the [13.5-16.6 at.%] range and a low Cu content up to 3.3 at.% (points 6 and 8, Figure 11d~~e~~). This phase exists only in contact with the interfaces with Al and brass whereas the center of the layer has not transformed as it remains composed of pure zinc (point 7, Figure 11d~~e~~).

Finally, concerning the chemical composition of the base materials on each side of the primitive Zn filler, not any diffusion of Zn was detected into brass while Zn has diffused into Al over a ~~close to 7 µm~~ distance close to 7 µm. This zone of penetration comprises a series of Al-based oversaturated solid solutions containing up to 3.5 at.% Zn.

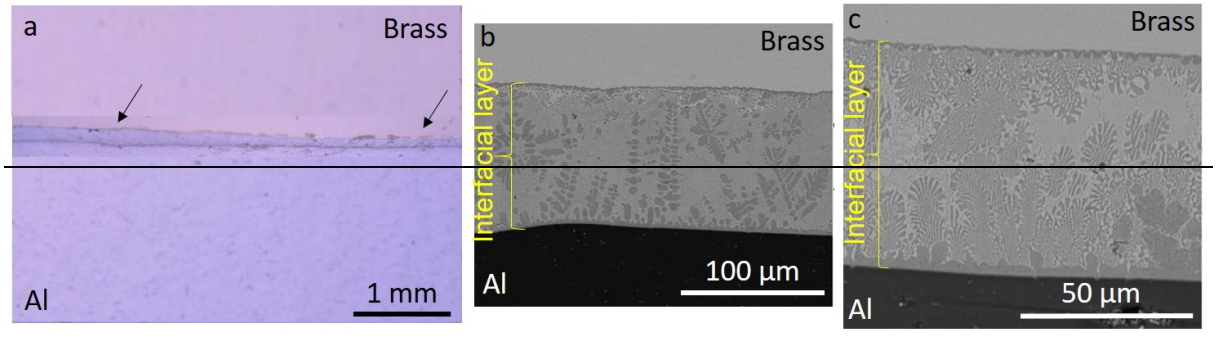

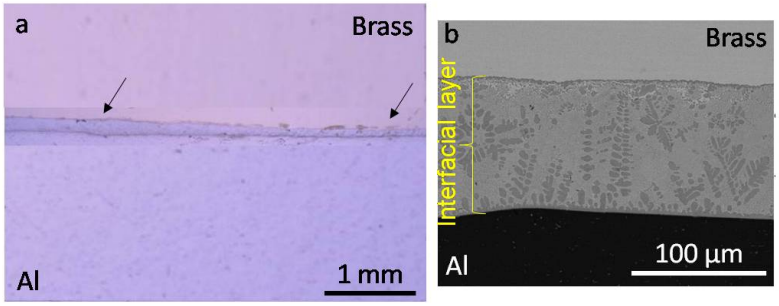

Figure 9: Micrographs of the interfacial zone below the tool contact area in the brass-Zn-Al joint (a: OM; b ~~and c~~: BSE/SEM).

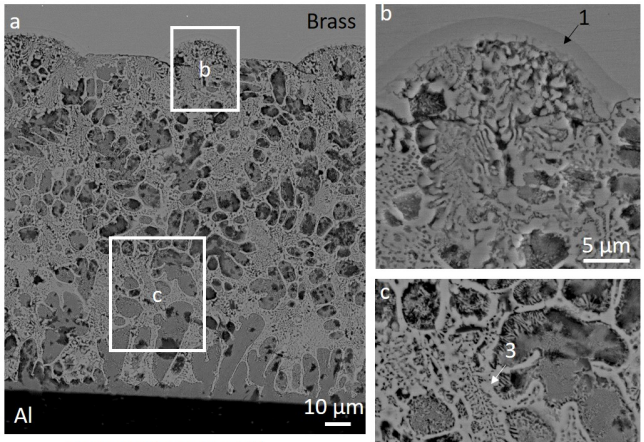

Compositions in at.%

Point	Al	Cu	Zn
1	13.2	41.9	44.9
2	48.9	5.6	45.6
3	11.0	11.8	77.1

Figure 10: Micrographs of the interfacial zone of the brass-Zn-Al joint along the weld just under the tool contact area (BSE/SEM) and EDX analyses.

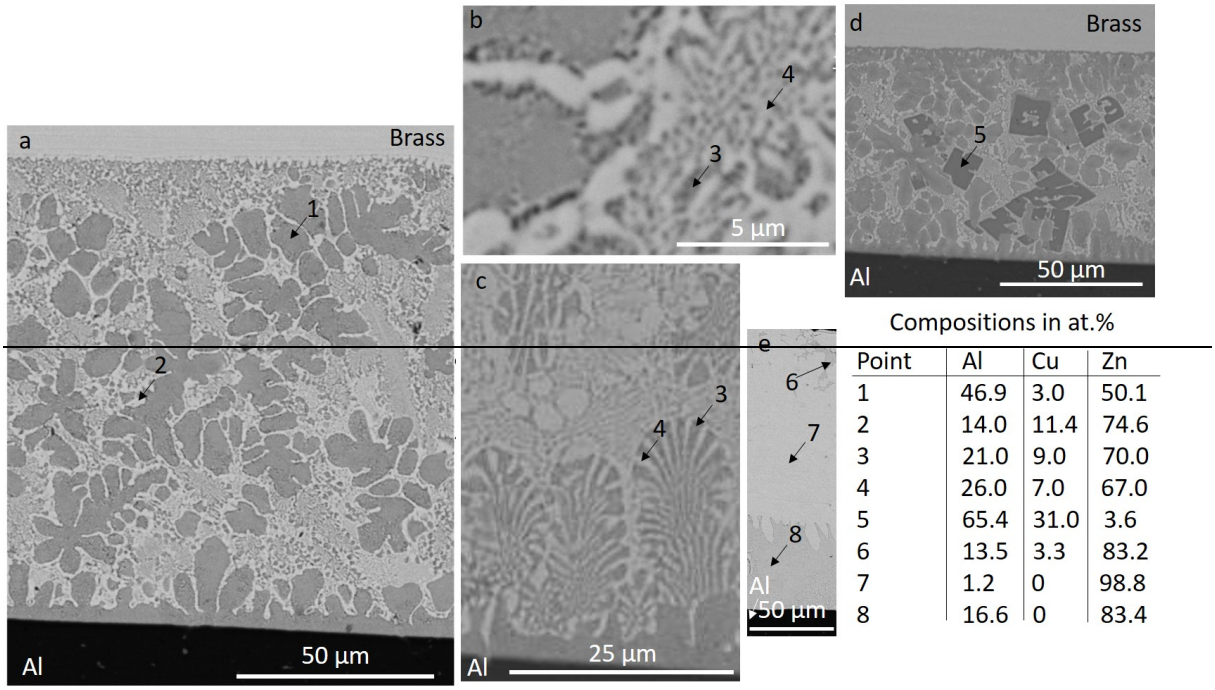

Compositions in at.%

Point	Al	Cu	Zn
1	46.9	3.0	50.1
2	14.0	11.4	74.6
3	21.0	9.0	70.0
4	26.0	7.0	67.0
5	65.4	31.0	3.6
6	13.5	3.3	83.2
7	1.2	0	98.8
8	16.6	0	83.4

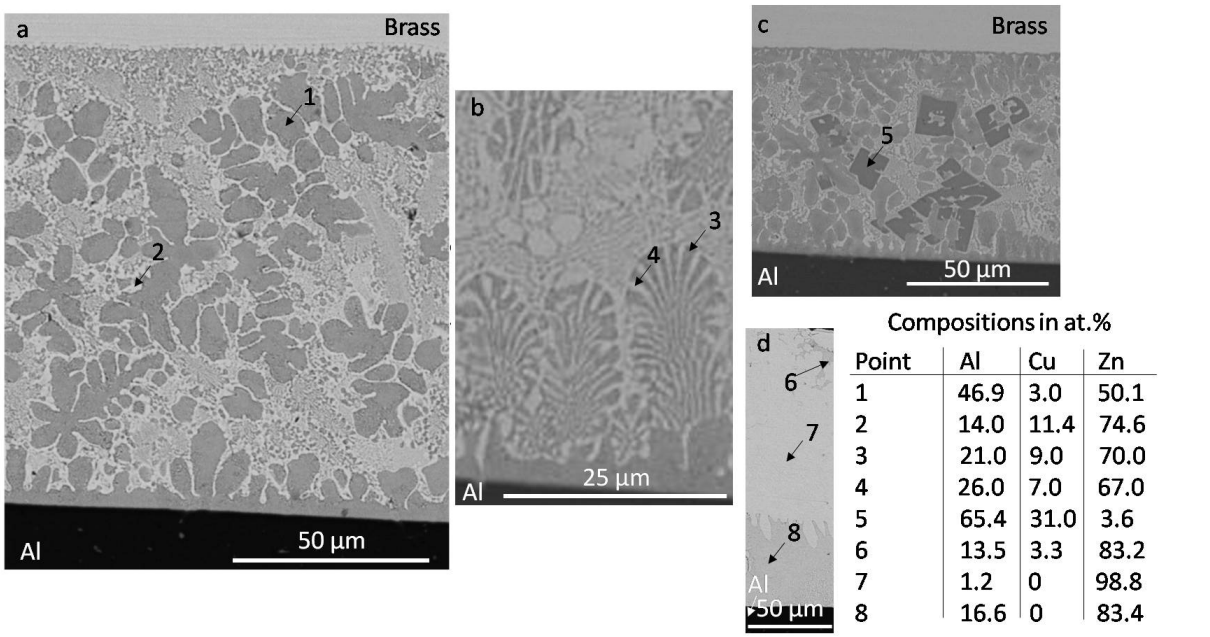

Compositions in at.%

Point	Al	Cu	Zn
1	46.9	3.0	50.1
2	14.0	11.4	74.6
3	21.0	9.0	70.0
4	26.0	7.0	67.0
5	65.4	31.0	3.6
6	13.5	3.3	83.2
7	1.2	0	98.8
8	16.6	0	83.4

Figure 11: Micrographs of the interfacial zone of the brass-Zn-Al joint (BSE/SEM) and atomic composition of the different phases (EDX/SEM).

3.3 Mechanical properties

Figure 12 shows that all the joints present low hardness zones in Al whatever its upper or lower position in the materials stacking. These soft zones supply information on the extent of the zones affected by heat and deformation in the (X-Y) transverse section. The softening in Al (figures 12a, b and c) is very likely due to dynamic recrystallization and grain growth because of the heat input more particularly brought in the top plate which was in contact with the tool. For the joints with Al at the top, the higher softening of Al in the Al-brass joint (figure 12c) can be linked to the higher peak temperature reached during welding (figure 4b). The high thermal diffusivity of Al and the low one of brass (table 2) are very likely responsible for the softening entailed by the heating of the brass bottom plate in the Al-brass

case (figure 12c). By way of contrast, the high thermal diffusivity of Al and Cu (table 2) led to no significant softening in the Cu bottom plate (figures 12a and b). Brass softening is far less marked in the brass-Zn-Al joint (figure 12d) very likely because of dynamic recrystallization as the peak temperature was clearly the highest one in this case (figure 4d). Besides, both the low thermal diffusivity of brass (table 2) and the high welding temperature are consistent with the softening of the Al lower plate in this joint (figure 12d).

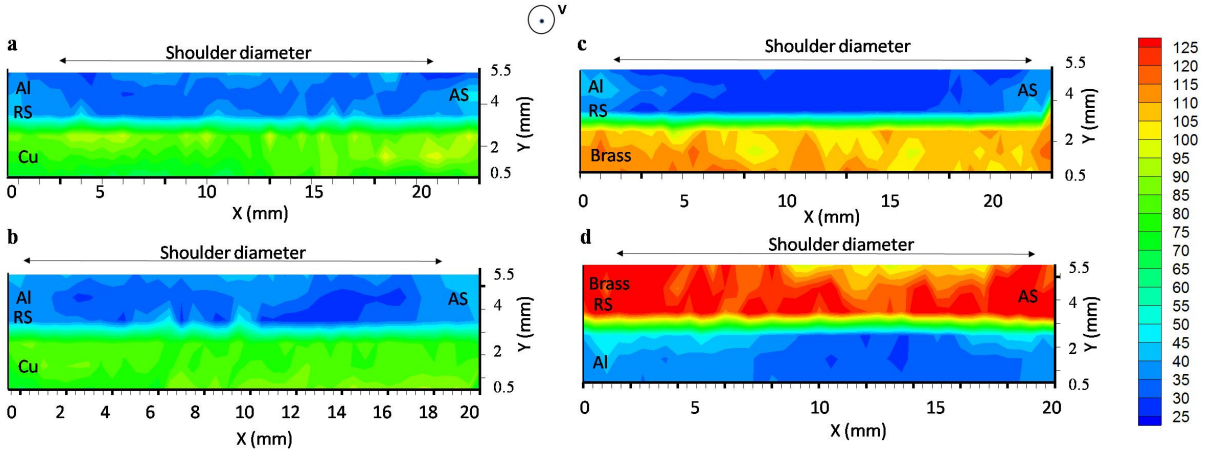

Figure 12: Vickers microhardness maps under 50 g of the Al-Cu (a), Al-Zn-Cu (b), Al-brass (c) and brass-Zn-Al (d) joints [(X,Y) transverse cross sections]. Zn and/or joint interface hardness was not evaluated. The light blue color in figures (a) and (b) and the green one in figures (c) and (d) at joint interfaces are meaningless since they are due to the signal treatment by the image analysis software. AS and RS stand for advancing and retreating side, respectively.

Figure 13 shows examples of the shear lap tensile curves for each kind of joints. These curves correspond to the fracture paths discussed in the following. The joints performances are actually erratic. The peak failure load, the total displacement and the fracture energy are low and in-between 156 and 2333 N, 0.8 and 5.6 mm, and 0.003 and 0.038 J/mm², respectively. The results are noticeably less dispersed with the brass-Zn-Al joint which is also the strongest and the most deformable.

Figure 14 depicts the global macroscopic aspect of the joints fracture surfaces, while figures 15-18 deal with their microscopic features. Except the case of the brass-Zn-Al weld which presents a chisel-type fracture of the Al base material, the other joints fail at the joint interface (figure 14).

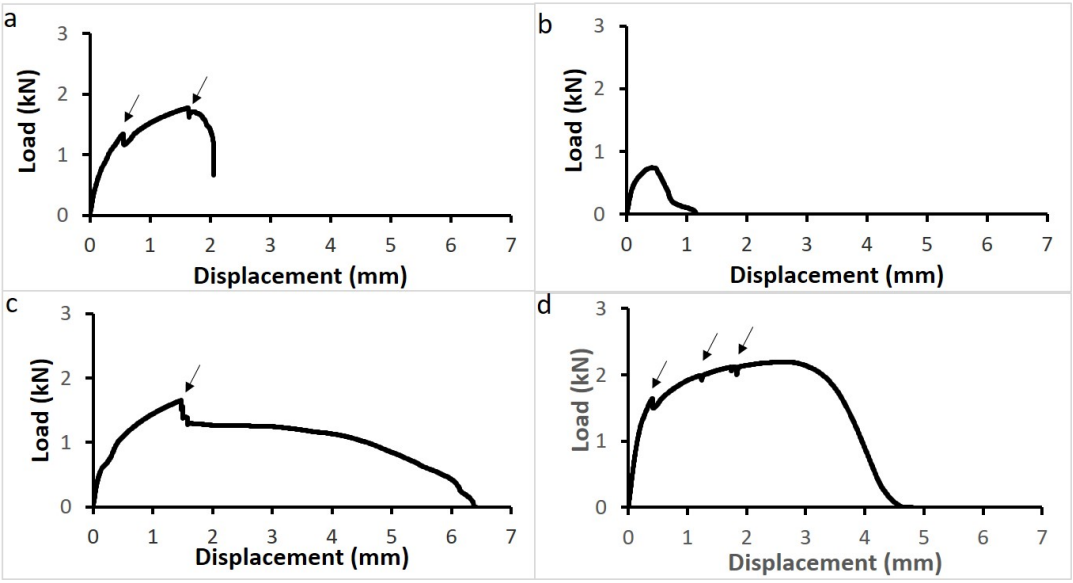

Figure 13: Examples of shear lap tensile curves of Al-Cu (a), Al-brass (b), Al-Zn-Cu (c) and brass-Zn-Al (d) joints.

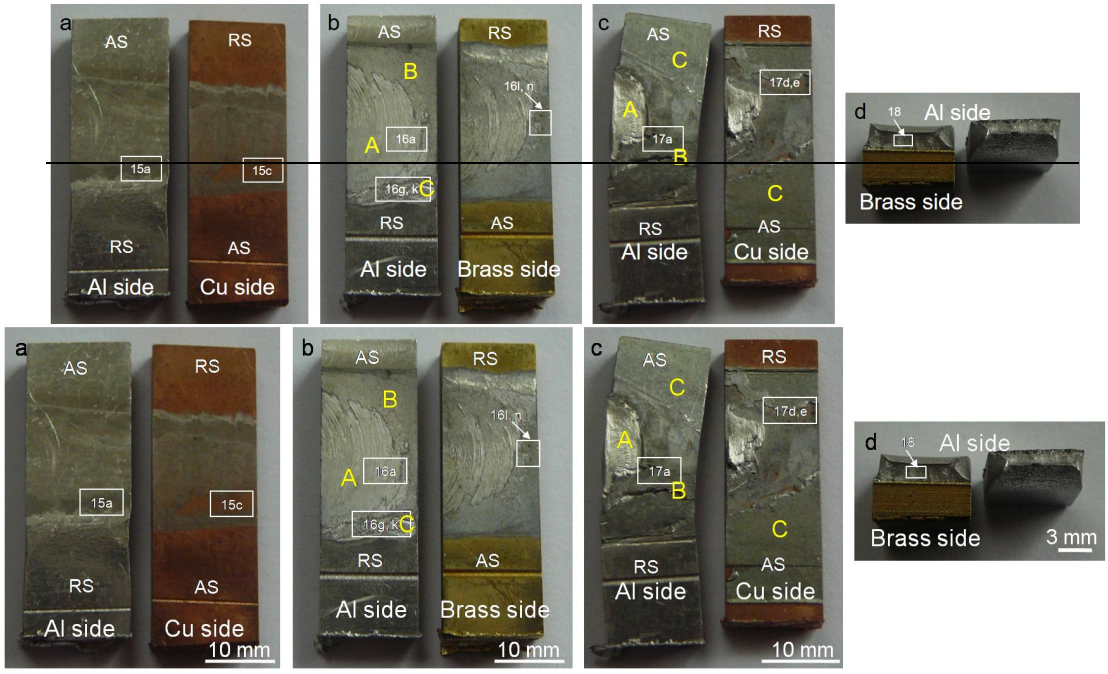

Figure 14: Global views of the Al-Cu (a), Al-brass (b), Al-Zn-Cu (c) and brass-Zn-Al (d) joint fracture surfaces. The boxes indicate the location of the fracture patterns enlargements. The corresponding micrographs are referred by their figure number in the present paper.

The shear tensile curve of the selected Al-Cu joint presents two transient drops of charge during loading. These discontinuities, noted by the dark arrows in figure 13a, are very likely due to the faint bonded areas self-evident by the changes of color visible on the fracture surface (figure 14a). In accordance with the shortness of the step of load diminution in figure 13a, figure 14a displays an incipient necking of the Al plate. Figures 14a and 15 further evidence that the Al-Cu joint has broken by shear along the interface. The fracture surfaces are pretty smooth on both sides (figure 15). They also contain some IMCs with a composition close to Al_2Cu (point 1), AlCu (points 2 and 3) and Al_2Cu_3 (point 4), among which some present cracks or interfacial decohesions are observed (yellow arrow in figure~~s~~ 15c ~~and 15d~~).

The IMCs compositions measured by EDX on the fracture surface are perfectly consistent with the results of the XRD analysis of the joint (figure 6).

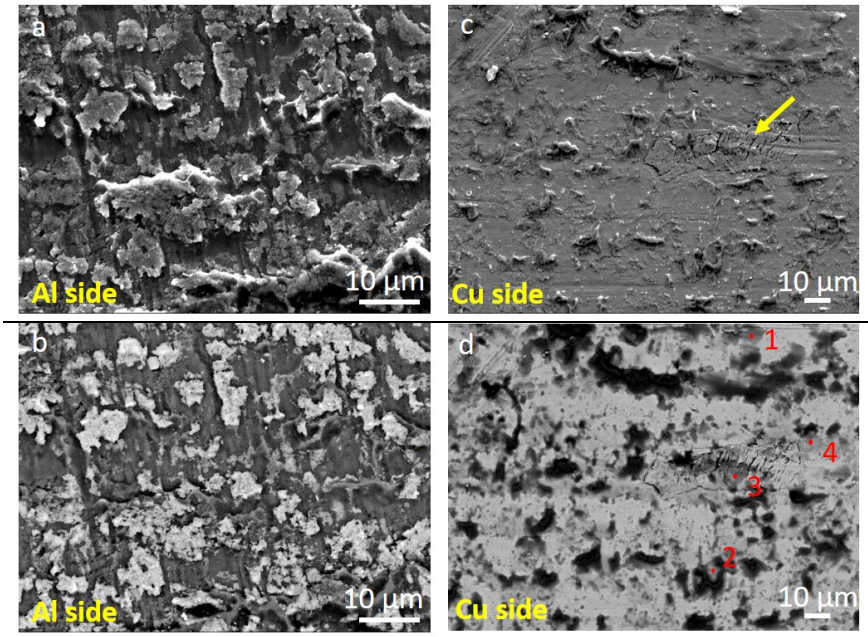

Compositions in at.%

Point	Al	Cu
1	64.4	35.6
2	49.2	50.8
3	55.9	44.0
4	41.9	58.1

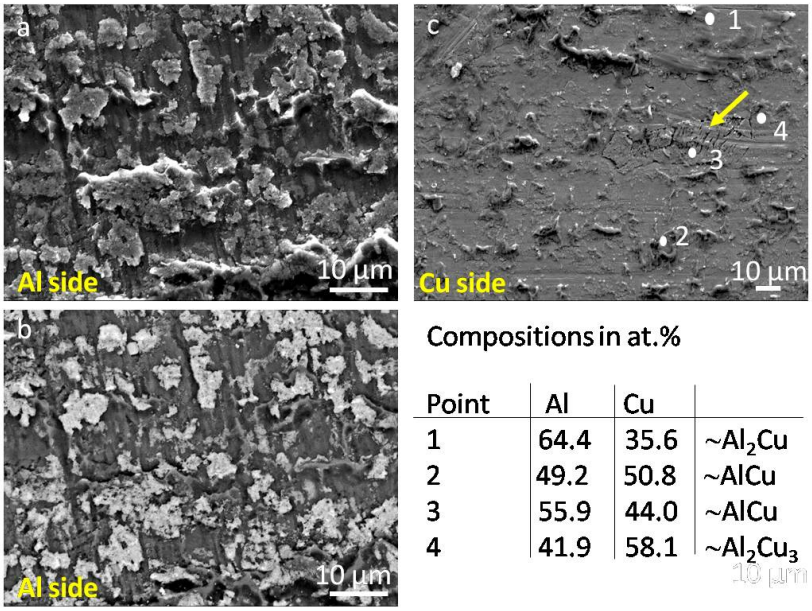

Compositions in at.%

Point	Al	Cu	
1	64.4	35.6	~Al_2Cu
2	49.2	50.8	~AlCu
3	55.9	44.0	~AlCu
4	41.9	58.1	~Al_2Cu_3

Figure 15: Fracture patterns of an Al-Cu joint: SE (a, c) and associated BSE (b~~, d~~) to (a) micrograph~~s~~, and EDX spot analyses. Cu appears brighter than Al with the BSE mode.

Concerning the selected Al-brass joint, Figure 13b corresponds to its worst mechanical behavior characterized by very low strength and ductility but with not any discontinuity along its load-displacement curve. A few load drops (not shown here) due to weld defects were on the contrary observed for the two other Al-Brass welds. The joint fractured once again within the interface (figure 14b). In this image, cracking very likely occurred by decohesion by shear in zone A which presents some circular traces of material flow. The crack then propagates by shear in the rather plane zone B and finally in zone C with final tearing. At a finer scale, whatever the side of the interface, some zones are indeed very flat (figures 16a and l) while others are rougher (figures 16g and n). The linear features displayed in figures 16a are part of

the semi-crowns visible in figure 14b. They remind the semi-crowns formed by a conventional pin tool **[24]**. In the current case, their presence can be questioned since FSW was performed with a pin free tool. The interfaces of the semi-crowns are enriched in Zn and 133 µm apart which corresponds to the welding pitch (advancing rate v divided by the rotational speed of the tool ω). In accordance with the results of the microstructural investigation of the joint interlayer (figure 7), numerous Al_2Cu compounds are found on each side of the fracture surface (points 1 in figure 16k and points 4 in figure 16c and n). Some of these intermetallics are clearly cracked (points 1 in figure 16k). On the brass side, the Cu-rich phases with compositions of points 2, close to the $Al_{4.2}Cu_{3.2}Zn_{0.7}$ (τ') stoichiometry, and of points 3 (γ-Cu_5Zn_8) (figures 16m and n) have also already been detected in the joint interlayer (figure 7). A mixture of Al and Zn based terminal solid solutions are moreover put into evidence on the Al side of the fracture surface (points 6 and 8 in figures 16b and c).

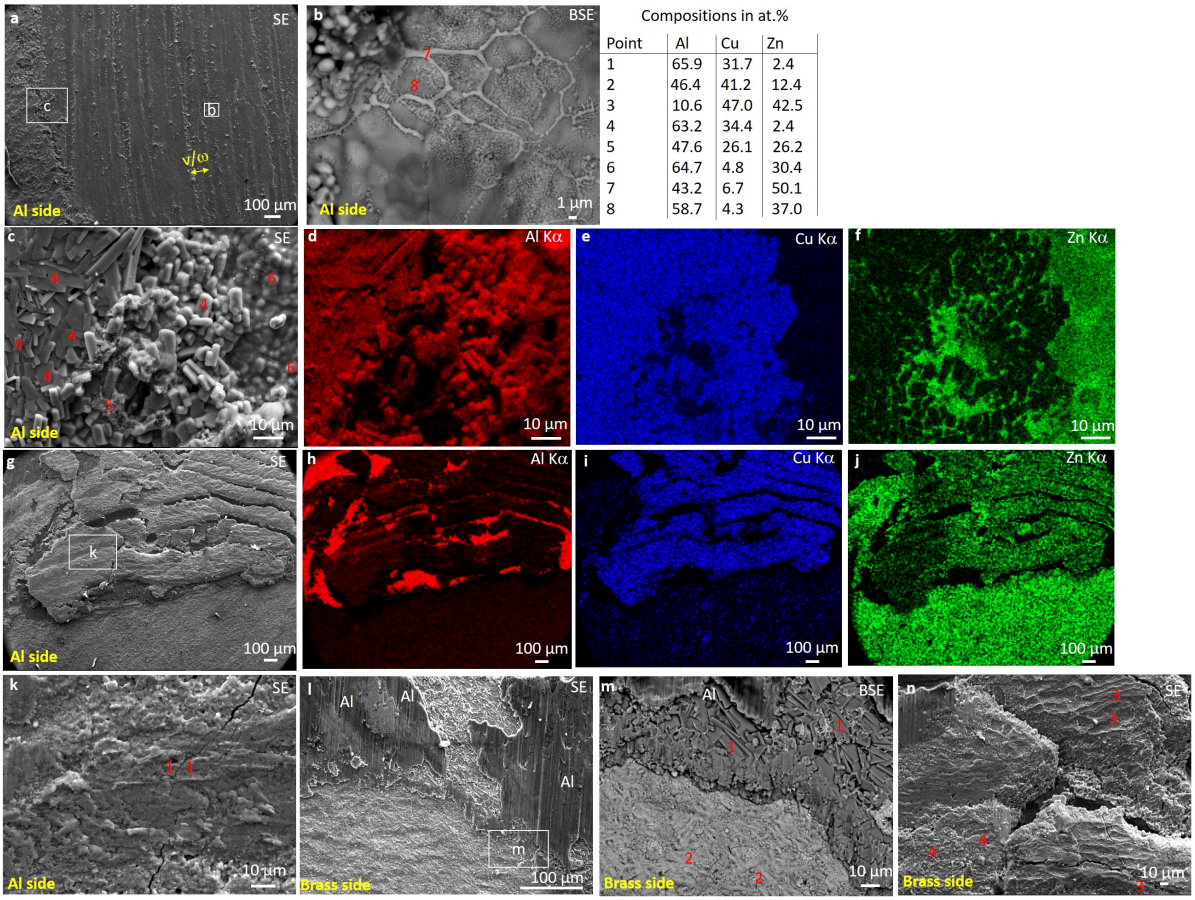

Figure 16: Fracture patterns of the Al-brass joint: details on 1) the Al side (a to k with d to f and h to j the X-ray maps associated to c and g, respectively) and 2) the brass side (l to n) with the EDX atomic compositions of different zones. Micrograph (m) is BSE analysis corresponding to part of (l) SE micrograph.

With regard to the Al-Zn-Cu joint kind, the selected sample is the most ductile of the three welds (figure 13c) which all failed at the joint interface. According to figure 14c which depicts the macroscopic fracture surface of this specimen, failure was very likely initiated by the cleavage cracking of remnant Zn in zone A because of the Zn brittleness at room temperature. This incipient fracture event corresponds to the load drop marked by the black arrow in the shear-tensile curve (figure 13c). Cracking pursued in zone B which was affected by areas of poor bonding particularly obvious on the Cu side (figure 14c). The deep Zn

bearing penetration paths in Al, already depicted in figure 8 and discussed in *§ 3.2 Joints structure*, are also cracked. This partial but already significant sample failure entails the bending of the more ductile Al plate during the final tearing of the joint by biaxial shear. This last step occurs in zone C (figure 14c). At a finer scale, figure 17 displays some features on both faces of the main crack. Whatever the Al or Cu side of the main crack, its surfaces are mainly smooth (figures 17 a, b, e and zone B in figure 14c) and Zn-rich. For instance, the eutectic-like lamellar zone in figures 17 a and b is composed of Al and Zn (figure 17c) as well as the smooth zone in figure 17 f which possesses a mean chemical composition close to that of an Al-Zn hypoeutectic material. This composition of points 4 has previously been found in the joint close to the Cu side (figure 8g). In accordance with the bonding of Al to Cu, both elements are also simultaneously present on both sides of the fracture path. Figure 17d, located in zone B in figure 14c, shows Al-rich debris whose ductile cracking arises from the shear elongation of their Cu substrate. On the other hand, EDX mapping clearly establishes the simultaneous presence of Cu and Zn in the extended flat areas visible on the Al side of the main crack (figures 17a and b). Besides, some Fe-bearing particles are also detected in the fracture surface (point 1 in figure 17 c). They are very likely stemming from the tool made of H13 steel which reveals some adhesive shoulder wear by an Al-Zn mixture. This observation is consistent with the good chemical affinity between Fe and both Al and Zn **[1]**. It also reminds the bad surface aspect of the Al-Zn-Cu joint (figure 5c) due to the materials sticking on the tool surface.

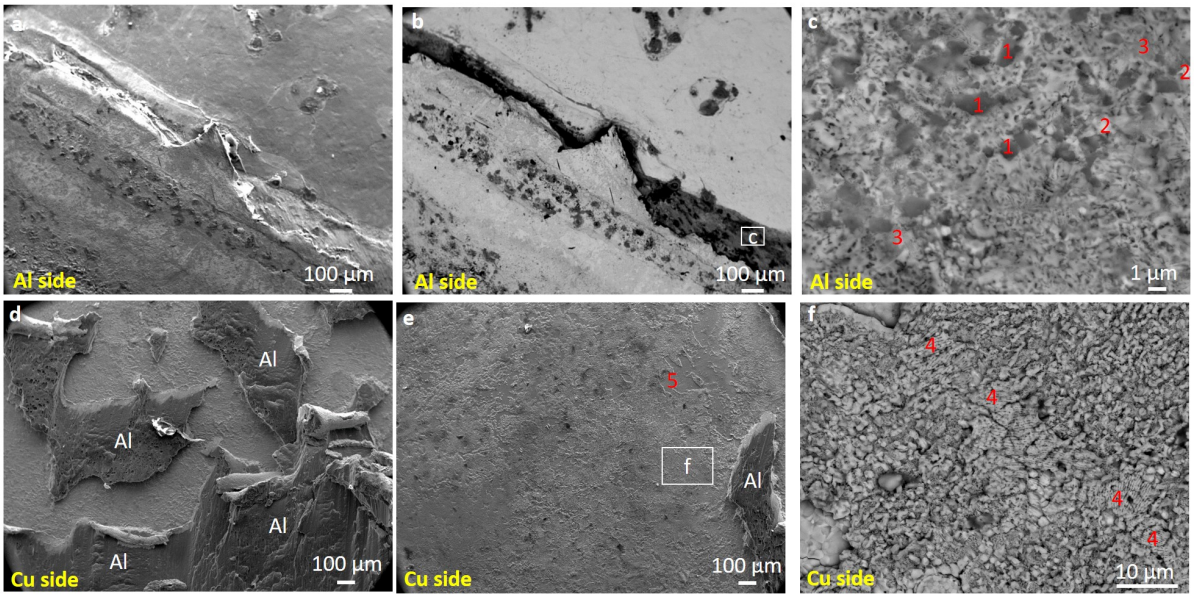

Compositions in at.%

Point	Al	Cu	Fe	Zn
1	78.1	0.1	10.6	11.2
2	58.3	0.0	1.5	40.2
3	66.5	0.0	0.4	32.2
4	17.1	7.8	0.0	75.1
5	1.5	48.6	0.0	49.9

Figure 17: Aspect of the fracture surface of the Al-Zn-Cu joint: SE micrographs (a, d, e) and associated BSE micrograph (b) of micrograph (a); c and f are magnifications of the b and e micrographs, respectively; EDX spot analyses. Cu is brighter than Al in the BSE mode.

At last, contrary to the other welds, and as exemplified in figure 13d, the load-displacement curves of the three brass-Zn-Al joints establish the occurrence of a significant elongation before a ductile mode of fracture. This elongation is however not perfectly uniform

as the consolidation is not continuous but suspended by few transient drops of charge (see black arrows in figure 13d). Despite this presence of weak points, and in accordance with the magnitude of the failure load, the final fracture has occurred by ductile necking of the Al base material (figures 14d and 18).

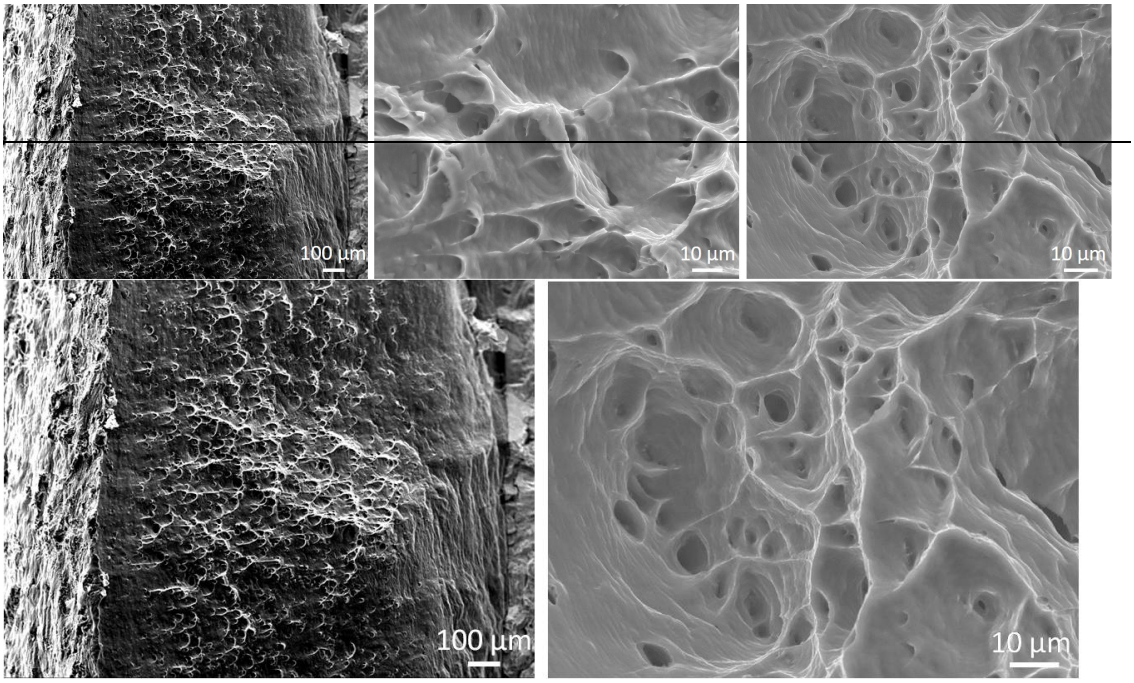

Figure 18: Ductile dimples on the Al fracture surface of a brass-Zn-Al joint (SE micrographs).

4. Discussion

4.1. Effect of pure Zn

The interposition of a pure Zn filler modifies the thermal exchanges, the material flow and the nature of phase transformations during welding.

Firstly, the differences between the welding thermal cycles of the Al-Cu and Al-Zn-Cu joints (figures 4a and c) can be explained by the change of thermal diffusivity of the various materials. In fact, according to table 2, Zn presents a far lower thermal diffusivity than both Al and Cu. Due to the interposition of a Zn layer at the faying interface which acts as a thermal barrier hampering the heat transmission to the bottom plate, the peak temperature measured beneath the sample is lower. The latter observation can also be explained at a lesser extent by the endothermal formation of Al-Zn eutectic phases (Figure 8).

Table 2: Physico-chemical properties of the different materials **[1]**.

Material	Brass C2600	Cu C1020	Zn	Al 1050
Melting temperature (°C)	950	1083	419.5	658
Density ($kg.m^{-3}$)	8500	8910	7140	2700
Specific heat ($J.kg^{-1}.°C^{-1}$)	375	393.5	388	945
Thermal conductivity ($W.m^{-1}.°C^{-1}$)	124	391.1	116	231
Coefficient of thermal expansion ($°C^{-1}$)	19.6×10^{-6}	17.3×10^{-6}	31×10^{-6}	23×10^{-6}
Thermal diffusivity ($m^2.s^{-1}$)	39×10^{-6}	111×10^{-6}	42×10^{-6}	90×10^{-6}

Secondly, the axial force applied on the tool during welding was smaller and much more erratic for the Al-Zn-Cu than for the Al-Cu joint (figures 4e and g). This difference clearly arises from Zn melting which facilitates the Al material flow in the bulk and causes

successive steps of sliding and sticking of the tool at the root surface in the Al-Zn-Cu case. In the Al-Cu case, tool traveling is on the contrary more difficult owing to the required plasticization of a totally solid phase.

Thirdly, as the Zn filler metal has melted, the interface temperature has reached, or overpassed, its 419.5°C melting point. At such a temperature, which corresponds to a homologous temperature of 0.75 for Al, Al is viscously deformed (figure 8). Concerning the phenomenological mechanism (figure 19c), once at the liquid state, Zn has very likely dissolved some Al to acquire the Al-Zn eutectic composition. Under the tool pressure effect, liquid Zn and/or Al-Zn eutectic were partially swept from the faying interface and engulfed by the Al viscous flow. These liquid phases with high fluidity were sucked up along the Al stream lines and through the whole Al plate thickness. Such an important extent of the Al flow lines up to the Al top surface is a priori disturbing according to the use of a pin free tool which should shear the upper plate at its contact only over a reduced depth compared to the 3 mm, and thus significant, plate thickness **[13,28]**. It very likely arises from the lubricant action of the liquid which facilitates the Al viscous flow. A similar penetration of Zn into Al up to the stirred surface has already been observed in presence of a Zn interlayer with the same thickness while using again a pinless tool but with a very likely higher heat input and only 2 mm thick plates **[29]**. Due to this liquid migration, Al grain boundaries liquation has sometimes occurred because of their eutectic transformation owing to their Zn enrichment by diffusion (figure 8l).

The chemical compositions of both phases in the eutectic, i.e. 67.3%Zn-31.7%Al-1%Cu and 87.7%Zn-8.9%Al-1.3%Cu (points 1 and 2, figure 8), are very likely somewhat erroneous because of the too large extent of the volume of analysis compared to the phases size. They are close to the equilibrium composition at the Al-Zn eutectic temperature **[1]**, as the apparent solubility of Cu in the eutectic phases remains very low (about 1 at.%). The mean composition of the eutectic constituent (figure 8) is also different from that of the equilibrium Al-Zn-Cu ternary eutectic point, namely 15.4% Al – 3.7%Cu – 80.9% Zn (at.%) at 377°C **[30]**. This discrepancy is suspected to result from an exacerbated undercooling owing to the high cooling rate. The present eutectic constituent also differs from

- the Cu-Zn rich compound and the 50%Al-46%Zn-4%Cu (at.%) ternary solid solution which formed at a lap joint interface obtained by using a pinless tool with the 1600 rpm / 40 mm/min and 1600 rpm / 20 mm/min, rotational and welding speeds, respectively **[29]**. The composition of the ternary alloy originates from a more important Zn-Al mixing than in the present case. Such a difference is consistent with the higher heat input due to the far lower welding speed than in the present study.

- the Al_4Cu_9, AlCu, Al_2Cu, $CuZn_2$, $CuZn_5$ and $CuZn_8$ IMCs developed in a lap joint made of a 2 mm thick Al top plate and of a 1 mm thick Cu bottom plate with a 50 µm thick Zn interlayer. This joint was obtained with a close to 2.1 mm of penetration of a pin tool rotating at 2500 rpm and advancing at 200 mm/min **[31]**. Such setting and configuration again give rise to both a higher heat input and a more efficient mechanical mixing than in the present study.

- the ternary eutectic, of unknown composition, and the Al_2Cu and $Al_{4.2}Cu_{3.2}Zn_{0.7}$ phases formed in an Al-Cu friction stir spot joint with a Zn interlayer obtained at 1400 rpm under an axial load of 1350 N applied to a pin tool **[32].**

- the $AlCu_3(Zn)$, $Al_2Cu_3(Zn)$, $Al_2Cu(Zn)$, $Al_4Cu_9(Zn)$ compounds observed in a lap friction stir brazed joint of 5 mm thick Al and Cu plates with a stepped configuration and a 0.1 mm thick Zn interlayer. Brazing was performed with a 30 mm diameter shoulder without pin and using the 1500 rpm and 750 mm/min rates **[12]**. In this case, the Al-Zn eutectic was expelled with oxides out of the interface, which permitted the formation of interfacial Al_xCu_y

IMCs. The IMCs layers were at most 4 µm thick and the joint fractured within the step portion of the Al plate but not at the faying interface.

At last, it is worth noting that no Zn has dissolved in pure Cu, while according to the Cu-Zn equilibrium phase diagram at 200°C about 35 at.% Zn can enter in solid solution in Cu to form α-brass **[1]**.

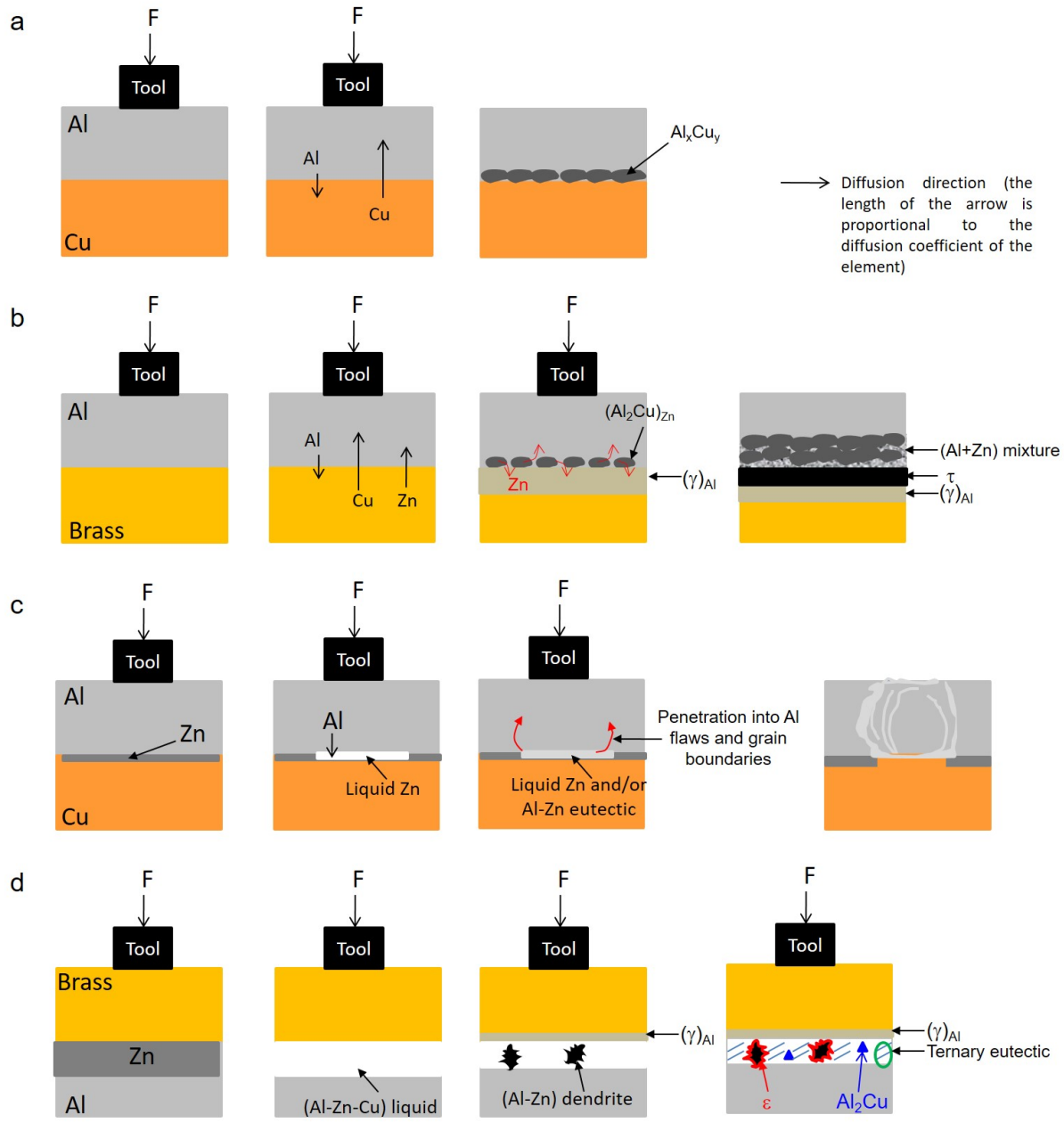

Figure 19: Phenomenological mechanisms of formation of the interface in the Al-Cu (a), Al-brass (b), Al-Zn-Cu (c) and brass-Zn-Al (d) joints. $(Al_2Cu)_{Zn}$ stands for an Al_2Cu phase with Zn in solid solution and $(\gamma)_{Al}$ for a γ phase with Al in solid solution. γ and τ are the abbreviations for the γ-Cu_5Zn_8 and the τ-$Al_{4.2}Cu_{3.2}Zn_{0.7}$ compounds, respectively.

Going to the Al-Cu joint, the atomic exchanges on the contrary occur at the solid state. They explain the formation of the Al_xCu_y discrete particles at the flat welding interface (figures 6 and 19a). No solidification trace, among which dendritic or eutectic structures, was

indeed observed. The interface peak temperature has thus remained below the 548°C equilibrium Al-Cu eutectic temperature **[1]**. So, supposing that the 340.5°C peak temperature measured at the Cu plate bottom corresponds to the interface temperature, the homologous temperature is 0.66 for Al and 0.45 for Cu. This difference of homologous temperature suggests that Cu diffuses preferentially into Al to form the Al_2Cu and AlCu, Al-rich compounds (figure 15). It can be guessed from the detection of the Al_4Cu_9 (figure 6) and Al_2Cu_3 (figure 15), Cu-rich compounds, that Al has also diffused into Cu. Indeed, and given the literature data which deals only with the 500°C temperature, the impurity diffusion coefficient of Cu in Al is four orders of magnitude higher than that of Al in Cu **[1]**. Moreover, always at 500°C, the diffusion coefficient of Al in an Al-3.05 at% Cu solid solution is 1.7×10^{-12} cm²/s whereas that of Cu is far higher and in-between 1.5×10^{-10} and 5.8×10^{-10} cm²/s in Cu-15 to 20.7 at.% Al alloys **[33]**. With the latter data and in case of a 10 s duration of welding at 500°C, the diffusion distance due to thermal agitation would be 0.4 to 0.8 µm for Cu into Al against the 0.04 µm far shorter distance covered by Al into Cu. The submicrometric size of the intermetallics observed at the interface (figure 6) is similar to the diffusion distance of Cu into Al at 500°C, which suggests that the formation of intermetallic compounds must result from thermal agitation assisted by deformation. Actually, the interfacial temperature is very likely lower than 500°C and rather close to the measured peak temperature under the Cu plate (figure 4) because of the excellent thermal diffusivity of Cu (tableau 2). Moreover, the analyzed intermetallic compounds already possess their equilibrium stoichiometry **[1]** which again supposes the efficiency of the lattice defects created by the plates deformation during welding so as to enhance atomic diffusion. With regard to the IMCs nature, the observation of Al_2Cu, Al_4Cu_9 and AlCu is consistent with experiments of chemical interdiffusion at an Al-Cu interface which put into evidence the nucleation of these three phases in this order **[34]**. The formation of Al_2Cu also agrees with the prediction of the effective heat of formation model according to which the first intermetallic phase to nucleate is the one with the most negative effective heat of formation at the composition of the lowest temperature of the liquidus **[35]**. According to this explanation, AlCu is the second one which should be formed followed by Al_4Cu_9. A comparison with the voluminous literature data showed that AlCu **[6,8,11,31,36-45]**, Al_2Cu **[2,5,6,8,11,31,36-55]**, Al_2Cu_3 **[39,42-44]** and Al_4Cu_9 **[2,5,8,31,36-43,45-47,49-55]** have already been observed in Al-Cu FSW joints obtained with pin tools and in various settings of processing such as linear friction stir welding or stationary friction stir spot welding with different welding and rotational speeds, joint configurations, tool morphology and dimensions, pin length, foil thickness...

4.2 Effect of Zn in solid solution in Cu.

This effect is deduced from the comparison between the Al-Cu and Al-brass joints. Zn in solid solution again modifies the thermal exchanges as well as the nature and spatial extent of the phase transformations (which take place this time essentially at the solid state) during welding.

Firstly, the higher thermal diffusivity of Cu, which entails a more efficient cooling of Cu compared to brass (table 2) explains that the force exerted on the tool to weld Al and Cu was greater than that used to weld Al and brass (figure 4), and all the more that α-brass is probably stronger than Cu at the welding temperature according to the open literature data. As aforesaid, it is indeed necessary to maintain a weld interface temperature adequate to ensure metallurgical bonding between both materials, given the lack of deformation of the weld interface in both cases.

Secondly, the difference of thermal diffusivity between brass and Cu (table 2) also contributes to the thicker interfacial area in the Al-brass joint than in the Al-Cu joint, namely

17 µm versus 80 nm up to 1 µm, respectively (figures 6 and 7). In fact, in spite of the slightly higher cooling rate for the Al-brass than for the Al-Cu joint (figure 4), more heat was kept at the Al-brass interface, which favored at the same time atomic diffusion and phases formation and growth.

Thirdly, whereas the Al-Cu joint interface was formed at the solid state, in the Al-brass case, partial melting is suggested to have taken place during welding according to the following comparison of the current analyses with the 400°C isothermal section of the Al-Cu-Zn equilibrium phase diagram (figure 20). Given, on the one hand, the high cooling rate, and on the other hand, the 371.4°C peak temperature for the Al-brass joint (figure 4b), which is lower than the joint interface temperature owing to the low thermal diffusivity (table 2), it seems relevant to compare the data of the equilibrium Al-Cu-Zn ternary phase diagram at 400°C, i.e. at a few higher temperature than 371.4°C, with the compositions of the analyzed zones in the Al-brass joint (figure 20). Figure 20 ascertains the existence of (i) a γ-Cu_5Zn_8 phase in close contact with brass (figure 7), (ii) $Al_{4.2}Cu_{3.2}Zn_{0.7}$ (τ') (figure 7 and point 2 in figure 16) and (iii) Al_2Cu (θ) (figure 7 and points 1 and 4 in figure 16). Concerning the phase transformations generating this interface (figure 19b), interdiffusion at first entailed the precipitation of Al_2Cu and γ phases polluted in Zn and Al, respectively. Then as Zn is almost insoluble in Al_2Cu, it was rejected by diffusion on either side of this phase. It then forms τ' in contact with the γ phase. Besides triphased domains comprising liquid, τ' and α-Al are expected to have transiently existed on the Al side according to the positioning of the compositions of points 5 and 7 in figure 16 on the Al-Cu-Zn equilibrium phase diagram (figure 20). This observation militates in favor of the formation of this joint in presence of liquid. No solidification feature is however obvious. The fact that welding would have proceeded at the liquid state, which favors atomic diffusion, is a second factor, and probably the salient one, which could explain the thicker interfacial area in the Al-brass case. Except Al_2Cu, the different phases identified in the Al-brass joint differ from the Al_4Cu_9 and CuZn compounds discovered in Al/brass FSW butt welds obtained with a pin tool **[56-58]**. The absence of Al_4Cu_9 phase at the present interface (figure 7) has to do with the precipitation of a continuous τ' layer which hinders the Al_4Cu_9 formation **[10,32,38]**.

It is worth noting that the Al-Cu and Al-brass joints both contain Al_2Cu particles at their interface (figures 7 and 15). This intermetallic compound still comprises a small amount of Zn, i.e. 2 to 4.6 at.% in the Al-brass case (figure 7). However, the solubility of Zn is very low, and close to 0.5 at.% in the Al_2Cu phase according to the ternary equilibrium phase diagram **[30]**. This remark suggests that the high cooling rate during welding (figure 4b) led to the formation of Al_2Cu oversaturated in Zn. Besides, the easy formation of Al_2Cu phase in the Al–brass joints can once again be explained by the very same arguments previously detailed for the Al-Cu case in the *§ 4.1 Effect of pure Zn* of the current discussion.

In addition, no extra diffusion of both Zn and Al into brass was detected and the composition of parent brass was unchanged during welding (figure 7).

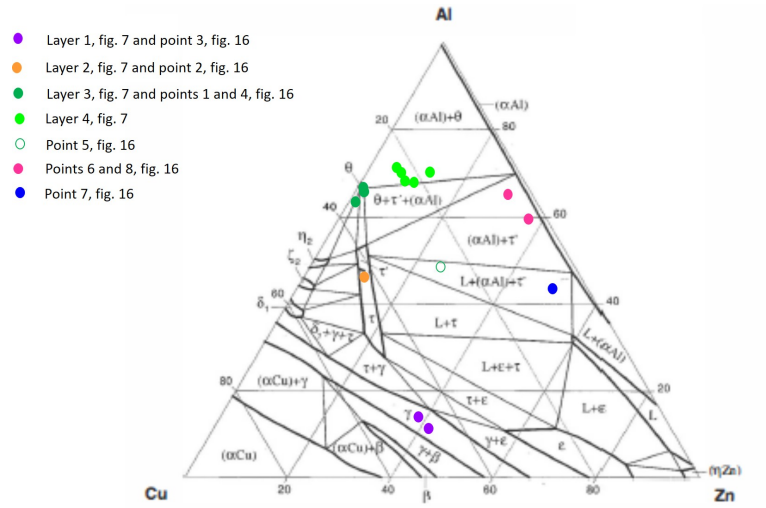

Figure 20: Positioning of the experimental compositions of the zones analyzed in the Al-brass joint (figures 7 and 16) on the 400°C isothermal section of the Al-Cu-Zn equilibrium phase diagram (at.%) **[30]**.

Both joints present low and erratic shear lap tensile properties (figure 13) and they fail in a brittle shear mode at areas of poor metallurgical bonding at the weld interface (figures 15 a and c and 16a and m). The fracture surfaces also present numerous zones of Al_2Cu cracking for both joints, while the τ' compound or some zones enriched in Al and Zn are also found in the fracture path of the Al-brass joint. The brittleness of the 3.9 GPa hard **[59]** Al_2Cu phases is indeed well known **[3]** whereas that of τ' is also clearly expected according to its 11.4 GPa **[10]** and thus very high hardness. The τ' brittleness however contrasts with some literature data **[32]** owing to the size dependence of the mechanical resistance of a brittle phase.

4.3 Brass-Zn-Al joint

For the brass-Zn-Al joint, as brass is stronger than Al at the welding temperature, a higher heat input was required to plasticize the top plate than with the other weld configurations with an Al top plate. It was ensured by both a higher tool rotational speed and a high axial force on the tool (figure 4h). As a result, the peak temperature, measured under the bottom plate, was significantly higher than with the other joints (figure 4d) despite the presence of a Zn interlayer, which was shown to play the role of a thermal barrier. Melting has occurred at the interface as proved by figures 9, 10 and 11, which exhibit dendrites of primary solid embedded in eutectic-like areas within an about 90 µm thick interface. The Al-Zn base composition of the dendrites (point 1, figure 11a) suggests that the liquidus temperature was close to 510°C according to the Al-Zn phase diagram **[1]**.

The phases compositions at the interface differ from the equilibrium ones **[30]**, because of the close to 14°C/s high cooling rate (figure 4d). Since the 477.6°C peak temperature measured underneath the joint during welding (figure 4d) is very likely lower than the true peak temperature because of the low thermal diffusivity of Zn, the experimental chemical compositions of the brass-Zn-Al joint have been reported on the liquidus surface of the Al-Cu-Zn equilibrium phase diagram (figure 21). Indeed, the chemical compositions measured at the solid state are in better agreement with this thermal projection than with the thermal section at 500°C, which can be explained by the high cooling rate during welding. Figure 21 is compatible with the dendrites composition which contain as much Al as Zn and a low Cu content; it also indicates that many compositions are very close to the ternary eutectic E3 composition where the L ↔ (Al) + ε + (Zn) reaction occurs at 377°C in equilibrium

conditions. Otherwise, the polygonal dark phase in figure 11dc was judiciously assimilated to an Al_2Cu phase oversaturated with 3.6 at.% Zn. Other measured compositions are contained in the primary ε phase domain. At last, the chemical composition at the brass-interlayer interface is contained in the primary γ phase domain on the liquidus surface.

With regard to the mechanism of formation of the brass-Zn-Al joint interface (figure 19d), first of all, Zn melting occurs and Al and Cu quickly dissolve in the liquid by diffusion. Some primary dendrites with equal contents of Al and Zn and only a few at% of Cu (point 1 [46.9%Al-3%Cu-50.1%Zn], figure 11) solidify at the interface, and the remaining liquid essentially enriched in Zn, Al and at a far lesser extent in Cu very likely undergoes a eutectic transformation; simultaneously, (i) a γ-Cu_5Zn_8 phase layer enriched in Al (point 1 [13.2%Al-41.9%Cu-44.9%Zn], figure 10) is precipitated on the brass side because of Zn and Al diffusion into brass; (ii) an ε phase is formed in the interdendritic spaces (point 3 [11%Al-11.8%Cu-77.1%Zn], figure 10, point 2 [14%Al-11.4%Cu-74.6%Zn], figure 11); (iii) the liquid locally enriched in Al and Cu at the interface led to the Al_2Cu phase precipitation (point 5, figure 11). In addition, at the interface far from the tool location, the composition of the E3 ternary eutectic leading to the formation of (Al), (Zn) and ε phases (points 6 [13.5%Al-3.3%Cu-83.2%Zn] and 8 [16.6%Al-0%Cu-83.4%Zn], figure 11) is locally reached.

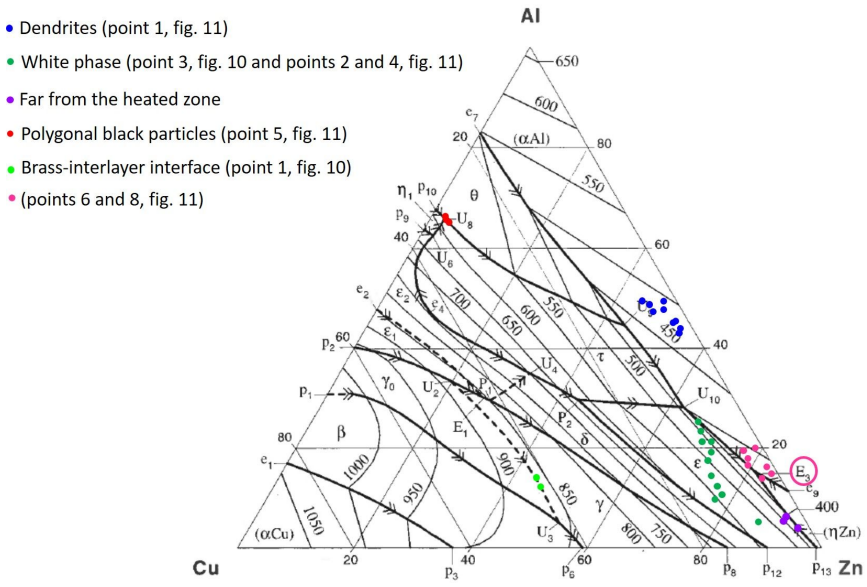

Figure 21: Overlapping of the experimental points of the analyzed zones of the brass-Zn-Al joint (figures 10 and 11) and of the liquidus surface (at.%) of the Al-Cu-Zn system **[30]**.

The present results differ from those reported by **[60]** in the case of the friction stir brazing of a 2.5 mm thick Al 6061 top plate with a 3 mm thick brass H62 (Cu-37.9wt.%Zn) bottom plate. Brazing was achieved by interposing a 0.1 mm thick Zn filler and using a 20 mm diameter pinless tool at the 1800 rpm and 60 mm/min speeds. Brazing generates a 16 µm thick interfacial layer comprising an Al and Zn bearing eutectic constituent as well as Al_4Cu_9, AlCu, CuZn, Cu_4Zn, $CuZn_5$, Al_2Cu, $Al_{4,2}Cu_{3,2}Zn_{0,7}$ intermetallic compounds. For this joint, the 480°C peak temperature registered at the joint interface **[60]** was similar to that recorded at the back of the present joint (figure 4d). In accordance with this result, and disregarding the difference of microstructure, the bonding interface thickness is thinner than the present one. The difference of interlayer thickness can very likely be explained by the present joint configuration which requires a higher heat input to plasticize the harder brass top plate and by the groove machined at the top of the bottom plate which enabled to trap liquid Zn at the joint

interface. In addition, the joint developed by Huang *et al* presents a tensile shear load of 7620 N for a bonding surface lower than 18×20 mm² **[60]** *vs.* 2300 N for a bonding area of 25×10 mm² in the present case, which proves that the weld developed by Huang *et al* with Al at the top is more performing regarding its mechanical resistance, very likely because of (i) its thinner interface and (ii) the more composite and miscellaneous aspect of its interfacial microstructure which contains additional IMCs such as Al_4Cu_9, CuZn and Cu_4Zn.

The present observations also differ from the microstructure of a 5052 Al alloy - brass butt joint laser brazed with a Zn - 15 at.% Al filler **[61]**. In this case, the interface was constituted, from brass to Al alloy, by a continuous CuZn layer, a continuous Al_4Cu_9 layer and by dendrites of the $Al_{4,2}Cu_{3,2}Zn_{0,7}$ phase embedded in solidified Zn-15 at.% Al **[61]**.

In spite of its thick interfacial layer, the brass-Zn-Al joint possesses the highest strength, ductility and fracture energy among all the tested joints. It fractures in the Al base material which is weaker than the joint interface (figure 13). The mechanical resistance of the thick interfacial layer contrasts with the brittleness of the few micrometers thick continuous interface of intermetallic compounds **[32]**. The difference very likely results from its composite and highly multiphased structure, composed of intermetallic compounds and eutectic, which is expected to hinder the cracks propagation.

4.4 Zn behaviour

Pure Zn acts as a thermal barrier. Indeed, because of its low thermal diffusivity (table 2), Zn concentrates heat at the faying interface, which entails Zn melting. The presence of liquid at the weld interface gives rise at first to the parent materials dissolution and subsequently to numerous phase transformations which are deleterious or beneficial for the joint mechanical behavior attending to the mechanical resistance of the top plate. If the upper plate is sufficiently strong to prevent stirring across its total thickness, and thus to hamper a marked Zn squeezing from its groove at the interface, sound joints are formed by friction stir brazing provided the reaction layer is not too thick. On the contrary, if stirring occurs through the whole thickness of the top plate, the Zn bearing liquid phases are expelled from the interface along the upper plate flow lines up to the top surface at the tool contact. As proved by the present work, such a Zn flow is expected to be harmful for the joint quality in case of a too heterogeneous stirring of the upper plate. The original thickness of the Zn filler and of the parent materials as well as the heat input and the mechanical behavior of the parent materials during welding must be tailored to obtain sound welds with the present process setup.

Owing to its effect on the heat exchanges, Zn in solid solution in α-brass also partially dissolves within Al to concentrate along unexpected semi crowns spaced by the welding pitch at the weld interface. Further work is underway in order to explain this puzzling feature.

4.5 Effect of the experimental setup

The present study shows that, with the selected process conditions, the used tool shape, namely pinless tool is not suitable for linear lap welding of thick plates. The material flow essentially limited to the top plate leads to an excessive flatness of the welding interfaces without any penetration of the top plate into the bottom plate. The lack of mechanical anchoring and the presence of unwelded areas explain the low shear resistance of the joints.

In the Al-Cu case, failure is aided by the discrete Al_xCu_y intermetallic particles located at the weld interface which are intrinsically brittle and act as points of stress concentration during the shear tensile test.

In the Al-Zn-Cu joint, the weld interface remained essentially flat because of the lubricant effect of Al-Zn eutectics. This liquid constituent has favored and generalized the

stirring across the whole thickness of the Al top plate, while this material flow was not markedly transmitted to the Cu bottom plate whose mechanical resistance is far higher than that of Al. In agreement with this deformation of the only top plate because of lubrication, the maps in figure 12 confirm the absence of microhardness evolution in the Cu bottom plate. The presence of both bulk islands and stream lines with high Zn concentrations (pure Zn or Al-Zn eutectics), with a significant notch effect owing to their acicular shape, both originate the brittle behaviour of the joint. The formation of these Zn rich zones resulting from (i) Zn trapping in the groove machined at the top of the bottom plate and (ii) a very heterogeneous and insufficient stirring should be avoided. This explains the harmful effect of Zn which contradicts number of literature data **[31,32]** concerned by a more homogeneous distribution of Zn generated by a more intense stirring. The deleterious effect of the trapping of liquid Zn bearing phases at the joint interface because of the groove is clearly established by the comparison of the present weld with an Al-Zn-Cu friction stir brazed joint **[12]**. In the latter experiment, 5 mm thick Al and Cu plates were also joined in lap stepped configuration using a 0.1 mm thick Zn filler and a pin free tool. It was reported that removal of oxide film on base materials surface occurred at the joint interface by rapid dissolution of the base materials into the molten Zn and by extrusion of excessive liquid out of the interface [**12**].

In the Al-brass case, the fracture surface is again essentially flat. There are however obvious signs of stirring (figures 16g and 16n) evidenced by lacks of adhesion and by the curious detection of crowns spaced by the twist pitch despite the use of a pinless tool, and whose borders are clearly enriched in Zn at least in Al (figures 16a and 16b). It reminds the present authors of observations in the literature where FSW with a 30 mm diameter pinless tool led to a lap joint of 2 mm thick Al and Cu plates in a stepped configuration with a 30 µm thick Zn interlayer. The Cu side of the latter joint fracture surface presented the adhesion of a small amount of pure Al along circular marks because of its previous melting **[12]**. The authors explained this phenomenon by a high torquing effect due to intense deformation under a high shoulder linear velocity and by an increase in total time under the torquing action **[12]**. Although less important, a similar effect could have happened in the present Al-brass joint where Zn contained in brass would have diffused and segregated at the joint interface and melt very locally. Complementary investigations are planned in order to elucidate the mechanism of formation of crowns at the interface. Nevertheless, their presence proves that, even if it was insufficient to alter the joint shape and to create a mechanical anchoring, the material flow generated by the tool was observed once again in the whole thickness of the Al top plate. Contrary to the Al-Zn-Cu case, the material transport in Al was not promoted by the marked presence of a liquid phase. Compared to the Al-Cu joint, it was nevertheless favored by the difference of mechanical resistance between the base materials and by the more important heat input (figure 4). Although it was not sufficient to lead to a suitable malleability of both materials at the interface location, the heating generated by the tool was however too important since it entailed the formation of an intermetallic layer with a thickness sufficient to cause the joint brittleness.

An eventual way of optimization could be an increase of the penetration depth **[62]** while adjusting the tool tilt **[63]** in order to maintain the surface features and to limit flash. But this way should increase the heat input with deleterious consequences on the IMCs formation. Another way of optimization would consist in changing the tool diameter **[19]** as well as the surface relief of the pinless tool **[17,64]**. For instance, the use of a fluted wiper tool instead of a flat featureless tool **[17]** is expected to embody the interface into the stirred zone and then to lead to the mechanical stirring of both parent materials. An increase of the tool diameter with its consequences on the torquing action and tangential forces as well as on the displacement (deformations, strains) at the joint interface can also generate the fracture of continuous IMCs layers, this cracking event prevailing on the harmful layers thickening due

to the heat input increase **[12]**. A heat input reduction caused by a decrease of the ratio between the rotational rate and the advancing speed with a pinless tool may also improve the mechanical properties of the joints, as shown by **[13]**.

Contrary to the Al-Zn-Cu case, Zn melting did not damage the root aspect (figure 5) and the soundness of the brass-Zn-Al weld (figures 13 and 14). This can be explained by the far higher mechanical resistance of the top plate which was not deformed over its whole thickness by the tool. As a consequence, the liquid phase was essentially trapped at the interface, which favored the interdiffusion phenomena and gave rise to a brazed joint. The mechanical resistance of this joint is due to metallurgical transformations and not to anchoring of the parent materials by interface deformations generated by the tool (figures 9, 10a, 11a and 11~~d~~c).

Dealing with the role of Zn during friction stir welding, the present results show that pure Zn acts as a thermal barrier. Indeed, because of its low thermal diffusivity (table 2), Zn concentrates heat at the faying interface, which entails its melting. As aforesaid, Zn melting may however be deleterious or favorable to the joint mechanical soundness according to the strength and chemical composition of the top plate.

Contrary to lots of literature data, either pure or in solid solution, Zn does not prevent the formation of the brittle Al_xCu_y intermetallic compounds, except in the Al-Zn-Cu joint, at least with the present experimental setup.

5. Conclusions

First attempts of linear friction stir lap welding between 3 mm thick plates of Al and either Cu or brass were performed with a pinless tool.

The process parameters were unsuitable so as to ensure the mechanical mixing of both plates owing to the welding interface flatness. In the case of an upper plate with a low mechanical resistance, melting of a Zn filler or formation of an Al-Zn eutectic are however able to promote stirring across the whole thickness of the top plate. On the contrary, in the case of an upper plate stronger than the bottom plate, liquid Zn remains trapped at the interface which gives rise to an efficient brazing. Zn melting is favored by its low thermal diffusivity.

The sweeping of liquid Zn along the Al flow lines acts as a marker for the material flow which was hitherto never investigated in the case of linear friction stir lap welding with a pinless tool.

Because at least of the low thermal diffusivity of brass, the Al-brass joint interfacial layer, which very likely formed at the liquid state and contains Al_2Cu, τ, γ phases and a mixture of Al and Zn terminal solid solutions, is thicker than the discrete Al_4Cu_9, AlCu, Al_2Cu and Al_3Cu_2 nanometer particles formed at the solid state at the Al-Cu joint interface.

With the used welding parameters, the presence of a Zn interlayer generated Al and Zn bearing dendritic structures and eutectics in both the Al-Zn-Cu and brass-Zn-Al joints. In the brass-Zn-Al welding interface, Al_2Cu, γ and ε phases were also formed while in the Al-Zn-Cu joint, eutectic and Zn penetration into the whole Al area heated by the shoulder were evidenced.

Owing to (i) the lack of mechanical anchoring, (ii) the occurrence of phase transformations and (iii) the presence of unbonded areas at the interface, all the joints, except the brass-Zn-Al one, have poor shear lap tensile properties. The crack nucleation effect of the Zn-rich flow lines has also been evidenced in the Al-Zn-Cu case. The fairly good mechanical behavior of the brass-Zn-Al weld is due to the complex composite nature of its rather thick interface.

Acknowledgments

The authors are very grateful to D. Troadec, IEMN, France for having performed thin foil cutting by FIB. The TEM facility in Lille (France) is supported by the Conseil Régional du Nord-Pas de Calais, and the European Regional Development Fund (ERDF). The authors thank the Chevreul Institute (FR 2638) for its help in the development of this work. Chevreul Institute is supported by the « Ministère de l'Enseignement Supérieur et de la Recherche », the « Région Nord-Pas de calais » and the « Fonds Européen de Développement des Régions ».

References

[1] Smithells Metal Reference Book, 7th ed., E.A. Brandes and G.B. Brook, eds., Oxford, U.K., 1992.

[2] Avettand-Fènoël MN., Taillard R., Ji G., Goran D. Multiscale study of interfacial intermetallic compounds in a dissimilar Al 6082-T6/Cu friction stir weld. Met Mat Trans A 2012; 43:4655-4666

[3] Avettand-Fènoël MN, Taillard R, Ji G. Quality of interfaces in Cu/Al dissimilar friction-stirred welds, Materials Science Forum, Thermec 2011, Québec 2012;706-709:959-964

[4] Solchenbach T., Plapper P., Cai W. Electrical performance of laser braze-welded aluminum-copper interconnects. J Manuf Proc 2014;16(2):183-189

[5] Zhang J., Shen Y., Yao X., Xu H., Li B. Investigation on dissimilar underwater friction stir lap welding of 6061-T6 aluminum alloy to pure copper. Mater Des 2014;64:74-80

[6] Muhammad NA., Wu CS., Tian W. Effect of ultrasonic vibration on the intermetallic compound layer formation in Al/Cu friction stir weld joints. J All Cpnds 2019;785:512-522

[7] Muhammad 2019b Muhammad NA., Wu CS. Ultrasonic vibration assited friction stir welding of aluminium alloy and pure copper. J Manuf Proc 2019;39:114-127

[8] Zhou L., Zhang RX., Li GH., Zhou WL., Huang YX., Song XG. Effect of pin profile on microstructure and mechanical properties of friction stir spot welded Al-Cu dissimilar metals. J Manuf Proc 2018;36:1-9

[9] Balasundaram R., Patel VK., Bhole SD., Chen DL. Effect of zinc interlayer on ultrasonic spot welded aluminum-to-copper joints. Mater Sci Eng A 2014;607:277-286

[10] Xiao Y., Ji H., Li M., Kim J. Ultrasound-assisted brazing of Cu/Al dissimilar metals using a Zn-3Al filler metal. Mater Des 2013;52:740-747

[11] Savolainen K., Mononen J., Saukkonen T., Hänninen H. A preliminary study on friction stir welding of dissimilar metal joints of copper and aluminium, FSW – TWI – 2006 – Paper 79

[12] Zhang GF., Zhang L., Zhang J., Zhang K. Approach to disrupting thick intermetallic compound interfacial layer in friction stir brazing (FSB) of Al/Cu plates. Sci Technol Weld Join 2014;19(7):554-559

[13] Simoncini M., Cicarrelli D., Forcellese A., Pieralisi M. Micro- and macro-mechanical properties of pinless friction stirred welded joints in AA 5754 aluminium thin sheets; International conference on Manufacture of Lightweight Components – ManuLight 2014, Procedia CIRP 18 (2014) 9-14.

[14] Schmidit H., Hattel J., Wert J. An analytical model for the heat generation in friction stir welding. Modell. Simul. Mater Sci Eng A 2004;121:43-57

[15] Tang W., Guo X., McClure JC., Murr LE. Heat input and temperature distribution in Friction Stir Welding, J Mater Proc Manuf Sci 1998;7:163-172.

[16] Kahraman F., Kahraman AD., Yolcu C., Gençer GM., Tüm M. Investigation of Microstructures and Mechanical Properties of the Joints which Welded by the Pinless Tool and the Designed Tool to Reduce the Keyhole in the Friction Stir Spot Welding, International Academic Conference on Applied Research in Engineering, Science & Technology Brussels, Belgium 14 th – 15 th September 2018

[17] Bakavos D., Chen Y., Babout L., Prangnell P. Material interactions in a novel pinless tool approach to friction stir spot welding thin aluminium sheet. Met. Mater. Trans. A 2011;42:1266-1282

[18] Kim KH., Bang HS., Bang HS., Kaplan AFH. Joint properties of ultra thin 430M2 ferritic stainless steel sheets by friciotn stir welding using pinless tool. J Mater Proc Technol 2017;243:381-386

[19] Forcelles A., Gabrielli F., Simoncini M. Mechanical properties and microstructure of joints in AZ31 thin sheets obtained by friction stir welding using “pin” and “pinless” tool configurations. Mater Des 2012;34:219-229

[20] Fuller C.B. Friction Stir Tooling: Tool Materials and Designs in Friction Stir Welding And Processing, R.D. Mishra and M.W. Mahoney Edts, ASM International, 2007

[21] Avettand-Fènoël MN., Nagaoka T., Fujii H., Taillard R. Characterization of WC/12Co cermet – steel dissimilar friction stir welds. J Manuf Proc 2018;31:139-155

[22] Avettand-Fènoël MN., Nagaoka T., Fujii H., Taillard R. Effect of a Ni interlayer on microstructure and mechanical properties of WC-12Co cermet / SC45 steel friction stir welds. J Manuf Proc 2019;40:1-15

[23] de Leon M., Shin HS. Material flow behaviours during friction stir spot welding of lightweight alloys using pin and pinless tools. Sci Technol Weld Join 2016;21(2):

[24] Avettand-Fènoël MN., Taillard R., Laye J., Odièvre T. Experimental investigation of three-dimensional (3D) material flow pattern in thick dissimilar 2050 friction-stir welds. Met Mater Trans A 2014;45:563-578

[25] Threadgill PL., Leonard AJ., Shercliff HR., Withers PJ. Friction stir welding of aluminium alloys. Intern Mater Rev 2009;54:49-93

[26] Arbegast WJ. Modeling friction stir joining as a metalworking process, Proceedings of Hot Deformation of Aluminum Alloys III. 2003:313–327

[27] Hetenyi M., McDonald PH. Contact stresses under combined pressure and twist. Trans ASME J Appl Mech 1958;25:396–401

[28] Cabibbo M., Forcellese A., Simoncini M. New Approaches to the Friction Stir Welding of Aluminum Alloys; Joining Technology, Chapter 2, Intech, 2016.

[29] Kuang B., Shen Y., Chen W., Yao X., Xu H., Gao J., Zhang J. The dissimilar friction stir lap welding of 1A99 Al to pure Cu using Zn as filler metal with 'pinless' tool configuration. Mater Des 2015;68:54-62

[30] Ghosh G., van Humbeeck J., Perrot P. Aluminium – Copper – Zinc, MSIT, Landolt-Börnstein, New Series IV/IIA2, 182-205

[31] Elerefaey A., Takahashi M., Ikeuchi K. Preliminary investigation of friction stir welding aluminium/copper lap joints. Weld World 2005;49(3/4):93-101

[32] Boucherit A., Avettand-Fènoël MN., Taillard R. Effect of a Zn interlayer on dissimilar FSSW of Al and Cu. Mater Des 2017;124:87-99

[33] Jost W. Diffusion in Solids, Liquids, Gases, E.M. Loebl, ed., Academic Press, New York, NY. 1960.

[34] Moreno D., Garrett J., Embury JD. A technique for rapid characterization of intermetallics and interfaces. Intermetallics 1999;7:1001–09.

[35] Pretorius R., Marais TK., Theron CC. Thin film compound phase formation sequence : an effective heat of formation rule. Mater Sci Eng R 1993;10:1–83.

[36] Xue P., Xiao BL., Ni DR., Ma ZY. Enhanced mechanical properties of friction stir welded dissimilar Al-Cu joint by intermetallic compounds. Mater Sci Engin A 2010;527:5723-5727

[37] Ouyang J, Yarrapareddy E, Kovacevic R. Microstructural evolution in the friction stir welded 061 aluminum alloy (T6-temper condition) to copper. J Mater Process Technol. 2006;172:110–122.

[38] Liu HJ., Shen JJ., Zhou L., Zhao YQ., Liu C., Kuang LY. Microstructural characterization and mechanical properties of friction stir welded joints of aluminium alloy to copper. Sci Technol Weld Join 2011;16(1):92-99

[39] Tan CW., Jiang ZG., Li LQ. et al. Microstructural evolution and mechanical properties of dissimilar Al–Cu joints produced by friction stir welding. Mater Des 2013;51:466–473.

[40] Muthu MFX, Jayabalan V. Tool travel speed effects on the microstructure of friction stir welded aluminum-copper joints. J Mater Process Technol 2015;217:105-113

[41] Kumar Sahu P., Pal S., Pal SK., Jain R. Influence of plate position, tool offset and tool rotational speed on mechanical properties and microstructures of dissimilar Al/Cu friction stir welding joints. J Mater Process Technol 2016;235:55-67

[42] Sinha VC, Kundu S, Chatterjee S. Microstructure and mechanical properties of similar and dissimilar joints of aluminium alloy and pure copper by friction stir welding. Perspectives in Science 2016;8:543-546

[43] Mubiayi MP., Akinlabi ET. Evolving properties of friction stir spot welds between AA1060 and commercially pure copper C11000. Trans Nonferrous Met Soc China 2016;26:1852-1862

[44] Fei X., Ye Y., Jin L., Wang H., Lv S. Special welding parameters study on Cu/Al joint in laser-heated friction stir welding. J Mater Process Technol 2018;256:160-171

[45] Mehta K., Badheka V.J. Influence of tool pin design on properties of dissimilar copper to aluminum friction stir welding. Trans Nonferrous Met Soc China 2017;27:36-54

[46] Akinlabi E., Els-Botes A., Lombard H. Effect of tool displacement on defect formation in friction stir welding of aluminium and copper, 8th international FSW symposium at Hamburg, Germany, May 2010:18-20

[47] Galvao I., Leal RM., Rodrigues DM., Loureiro A. Dissimilar welding of very thin aluminium and copper plates, 8th international FSW symposium at Hamburg, Germany, May 18-20, 2010

[48] Ivanov E., Theado E. Full surface friction stir welding of aluminium 7075 alloy to copper, 8th international FSW symposium at Hamburg, Germany, May 18-20, 2010

[49] Genevois C., Girard M., Huneau B., Sauvage X., Racineux G. Interfacial reaction during friction stir welding of Al and Cu. Metall Mater Trans A 2011;42(8):2290-2295.

[50] Xue P., Ni DR., Wang D., Xiao BL., Ma ZY. Effect of friction stir welding parameters on the microstructure and mechanical properties of the dissimilar Al-Cu joints. Mater Sci Engin A 2011;528:4683-4689

[51] Galvao I., Verdera D., Gesto D., Loureiro A., Rodrigues D.M. Influence of aluminium alloy type on dissimilar friction stir lap welding of aluminium to copper. J Mater Process Technol 2013;213:1920-1928

[52] Barekatain H., Kazeminezhad M., Kokabi AH. Microstructure and mechanical properties in dissimilar butt friction stir welding of severely plastic deformed aluminum AA1050 and commercially pure copper sheets. J Mater Process Technol 2014;30(8):826-834

[53] Zhang W., Shen Y., Yan Y., Guo R. Dissimilar friction stir welding of 6061 Al to T2 pure Cu adopting tooth-shaped joint configuration: microstructure and mechanical properties. Mater Sci Eng A 2017;690:355-364

[54] Khojastehnezhad VM., Pourasl HH. Microstructural characterization and mechanical properties of aluminum 6061-T6 plates welded with copper insert plate (Al/Cu/Al) using friction stir welding. Trans Nonferrous Met Soc China 2018;28:415-426

[55] Tavassolimanesh A., Nia AA. A new approach for manufacturing copper-clad aluminum bimetallic tubes by friction stir welding (FSW). J Manuf Proc 2017;30:374-384

[56] Esmaeili A., Zareie Rajani HR., Sharbati M., Besharati Givi MK., Shamanian M. The role of rotation speed on intermetallic compounds formation and mechanical behavior of friction stir welded brass/aluminum 1050 couple. Intermetallics 2011;19:1711-1719

[57] Esmaeili A., Besharati Givi MK., Zareie Rajani HR. A metallurgical and mechanical study on dissimilar friction stir welding of aluminum 1050 to brass (CuZn30). Mater Sci Eng A 2011;528:7093-7102

[58] Akbai M., Behnagh RA. Dissimilar friction-stir lap joining of 5083 aluminum alloy to CuZn34 brass. Metall Mater Trans B 2012;43:1177–1186.

[59] Gilman JJ. Chemistry and Physics of Mechanical Hardness, Wiley and sons Edt, New Jersey, 2009.

[60] Huang G., Feng X., Shen Y., Zheng Q., Zhao P. Friction stir brazing of 6061 aluminum alloy and H62 brass: evaluation of microstructure, mechanical and fracture behavior. Mater Design 2016;99:403-411

[61] Zhou L., Li ZY., Song XG., Tan CW., He ZZ., Huang YX., Feng JC. Influence of laser offset on laser welding-brazing of Al-brass dissimilar alloys. J All Cpnds 2017;717:78-92

[62] Tozaki Y., Uematsu Y., Tokaji K., A newly developed tool without probe for friction stir spot welding and its performance, J Mater Proc Technol, 2010;210:844-851

[63] Dialami N., Chiumenti M., Cervera M., de Saracibar C.A. A fast and accurate two-stage strategy to evaluate the effect of the pin tool profile on metal flow, torque and forces during friction stir welding. Int. J. Mech. Sci. 2017;122:215–227

[64] Ji S., Meng X., Ma L., Gao S.S., Effect of groove distribution in shoulder on formation, macrostructures, and mechanical properties of pinless friction stir welding of 6061-O aluminum alloy, Intern J Adv Manuf Technol 2016;87:3051-3058